Distance Learning Operations Course

IC 5.7: Convective Storm Structure and Evolution

Presented by the Warning Decision Training Branch

Version: 0110.1

IC 5.7: Convective Storm Structure and Evolution

Table of Contents

IC 5.7: Convective Storm Structure and Evolution ii

Table of Contents ii

Lesson 1: Introduction 1

Objectives 2

Lesson 2 2

Lesson 3 2

Lesson 4 2

Lesson 2: Fundamental Relationships Between Shear and Instability on Convective Storm Structure and Type. 4

Objective 1 4

Effects of Shear 4

Objective 2 5

Objective 3 8

Midlevel Dry Air Promotes Stronger Downdrafts 8

Effect on Storm Evolution Due to Vertical Placement of Dry Midlevel Air 9

Downdraft Convective Available Potential Energy (DCAPE) 10

Dichotomous Effects of Dry Midlevel Air 11

Rules of Thumb for Mean Relative Humidity (RH) 11

Inverse Relationship Between DCAPE and Mean Winds in Estimating Cold Pool Strength 12

Objective 4 12

Objective 5 14

Lesson 3: Definitions, Strengths, and Limitations of Environmental Parameters 16

Objectives 6 - 8 16

Buoyancy 16

Shear 19

Storm Relative Helicity (SRH) 21

Midlevel Flow in Tornadic and Nontornadic Storms 24

Shear and Buoyancy Combinations 25

Summary 28

Lesson 4: Propagation and Evolution of Convection 31

Objective 9 31

Objective 10 32

Straight Hodograph Dynamic Processes 32

Curved Hodographs 35

Other Propagation Forces 38
Objective 11 38
The Old Supercell Motion Method 38
The Internal Dynamics (ID) Method 39
Magnitude of Deviant Motion and Other Issues 41
Objective 12 42
Multicell Storm Propagation 42
Shear-cold Pool Interactions 43
Gradients in Instability 46
System-relative Low-level Flow 47
Boundary Interactions With Other Boundaries or Topography 49
More Than One Propagation Mechanism at Once 51
Objective 13 51
The Role of Convective Instability 52
Vertical Wind Shear Effects and Relationship With CAPE in Squall Line Systems. 53
Role of Deep-layer Shear 57
Inverse Relationship Between CAPE and Shear 59
Objective 14 59
Definition of a Rear-Inflow Jet (RIJ) 60
A Brief Backround 60
The Dynamics of an RIJ 61
Descending vs. Nondescending RIJs 64
Other Mechanisms Leading to Long-lived Damaging Squall Lines 66
Objective 15 67
Line-end Vortices 67
Characteristics of Severe Bow Echoes 70
Mechanisms Leading To Line-end Vortex Formation 76
Summary 79
Motion of Convection 80
Multicell Longevity 80
RIJs 81
Bow Echoes 81

Appendix A: References 83

Appendix B: Bibliography 89

Lesson 1: Introduction

Instructional Component 5.7 covers the fundamentals of convective storm structure and evolution. The first lesson is devoted to describing the basic relationships between shear and instability with respect to convective storm type. The next lesson treats some of the more commonly used parameters for forecasting convective storm type and movement. The final lesson discusses the evolution and associated morphologies of storm types with emphasis on multicell systems.

Although this is an expansive subject, it is crucial to understanding how radar and other sensor data can be effectively used in the warning process. There are several subcomponents to this IC including:

- *Anticipating Convective Storm Structure and Evolution* CD module (COMET 1996)
- *A Convective Storm Matrix* CD module (COMET 1995)
- *Mesoscale Convective Systems: Squall Lines and Bow Echoes* online module (COMET 1999) (http://meted.ucar.edu/convectn/mcs/).
- This student guide
- The teletraining session

This student guide is designed to summarize and review the major objectives covered in the COMET modules, developed from 1995-1999. The student guide also incorporates new scientific findings related to convective storm structure and evolution. A prerequisite for IC 5.7 is RTM-230. RTM-230 is a training module containing basic

information on sounding analysis. It is available for download from the NWS Training Center at:

`ftp://ftp.nwstc.noaa.gov/d.MET/RTM-230.EXE`

Objectives

The following are the specific objectives for IC 5.7:

Lesson 2 Fundamental Relationship of Shear and Instability on Convective Storm Structure and Type.

1. For a given quantity of buoyancy, determine the influence of shear strength on overall storm structure and evolution.
2. For a given hodograph and magnitude of vertical wind shear, identify the influences of variations to the buoyancy profile on overall storm structure and evolution.
3. For a given hodograph and magnitude of vertical wind shear, describe the role of midlevel dry air on storm evolution.
4. Explain the role of shear depth in controlling the resulting storm structure and evolution.
5. Explain the role of hodograph curvature in controlling resulting storm structure and evolution for strongly sheared environments.

Lesson 3 Definitions, Strengths, and Limitations of Parameters Used for Forecasting Severe Weather Type

6. Identify definitions, strengths, and limitations of some of the most operationally relevant kinematic and thermodynamic parameters for forecasting convective storm type.
7. Identify the physical process associated with the convective storm parameters listed in Objective 6.
8. Describe the basic relationships between shear and instability in forecasting severe storm type.

Lesson 4 Evolution and Morphology of Convective Storms

9. Describe the physical mechanisms that determine the motion for ordinary cells.
10. Describe the physical mechanisms that determine the motion for supercell convection.
11. Describe ways to estimate supercell motion from a hodograph.
12. Describe the physical mechanisms that determine the motion of multicell convection.
13. For multicell convection, describe how interactions with the near-storm environment affects its longevity.
14. Describe the role of the Rear-Inflow Jet (RIJ) in squall line intensity.
15. Identify the characteristics of bow echoes and the mechanisms involved in their formation.

Lesson 2: Fundamental Relationships Between Shear and Instability on Convective Storm Structure and Type.

Objective 1

For a given quantity of buoyancy, determine the influence of shear strength on overall storm structure and evolution.

Based on observations and modeling studies, the organization and longevity of convective storms and storm systems tend to increase with increasing magnitudes of vertical wind shear. For example, ordinary cells tend to occur at the weakest end of the shear spectrum, while supercell environments generally possess some of the strongest values of shear. Figure 2-1, from the COMET CD-ROM, *A Convective Storm Matrix*, illustrates the integrated effects of vertical wind shear on the spectrum of convective storm processes.

Effects of Shear

Generally speaking, the longer the hodograph (length), the more vertical shear (and subsequent horizontal vorticity) will be present in the atmosphere. Increasing vertical shear creates more opportunities for storms to develop midlevel rotation in their updrafts. Another effect of vertical wind shear, due to horizontal pressure gradients induced from vertical shear and a blocking updraft column, is that a convective cloud will become tilted in the direction of the vertical shear vector. This tilting acts to distribute rainfall downshear from the updraft, which is a detrimental influence to storm longevity.

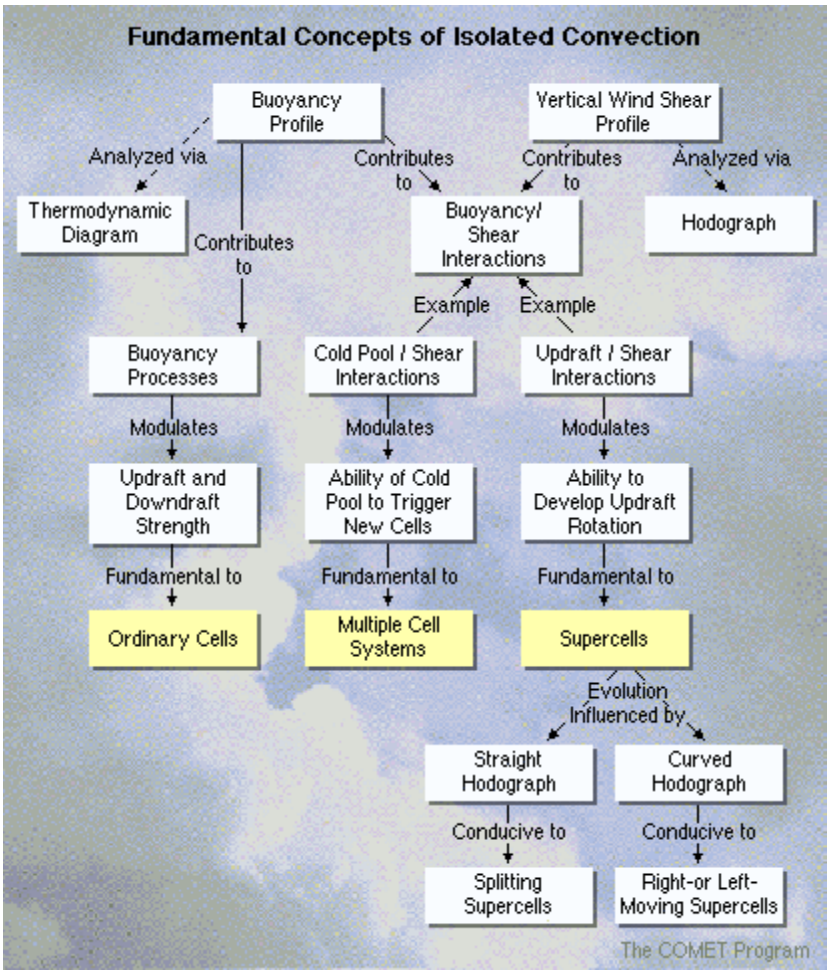

Figure 2-1. A schematic flowchart showing the fundamental concepts of convection. From *A Convective Storm Matrix* (COMET 1995).

Objective 2

For a given hodograph and magnitude of vertical wind shear, identify the influences of variations to the buoyancy profile on overall storm structure and evolution.

Increasing the buoyant energy in a convective storm or system tends to increase the size, depth, and strength of the individual convective cells, and the overall size and strength of the whole convective system. The amount of buoyancy and shear in the environment helps determine storm type. A depiction of the relationship between shear and buoyancy in numerically simulated storms is

shown in Figure 2-2. The general relationship between buoyancy as expressed by Convective Available Potential Energy (CAPE), and Storm-Relative Helicity (SRH), in observations of tornado proximity soundings (Fig. 2-3) are somewhat similar to the numerical modeling results shown in Fig.

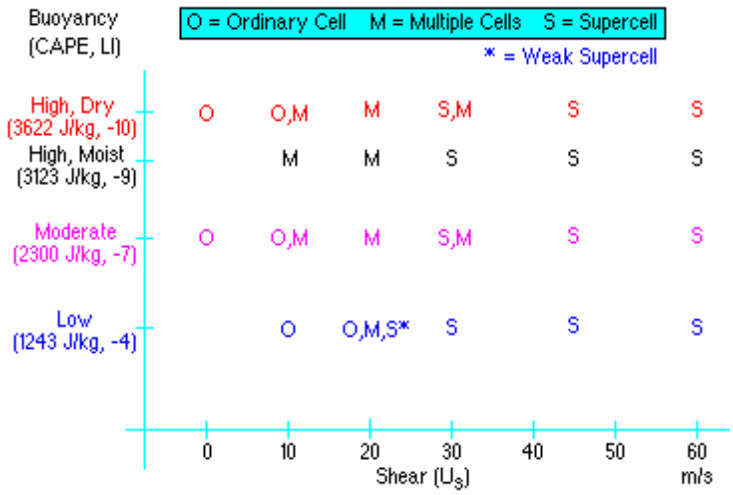

Figure 2-2. Distribution of buoyancy (CAPE, Lifted Index) and shear (hodograph length - U_S) for 3 classes of storms in numerical model simulations from *A Convective Storm Matrix* (COMET1995).

2-2. Edwards and Thompson (2000) suggested that increases in CAPE have a stronger influence on tornado likelihood than 0-3 km SRH, with SRH displaying a wider distribution of values for lower CAPE values in nontornadic events (Fig. 2-3). Johns et al. (1990) indicated a broad range of possible CAPE and SRH (0-2 km) combinations for F2 and greater tornado proximity sounding cases (Fig. 2-4). There are some general relationships that can be gathered from these studies:

- Increasing shear in a high CAPE environment can increase the probability of supercells.

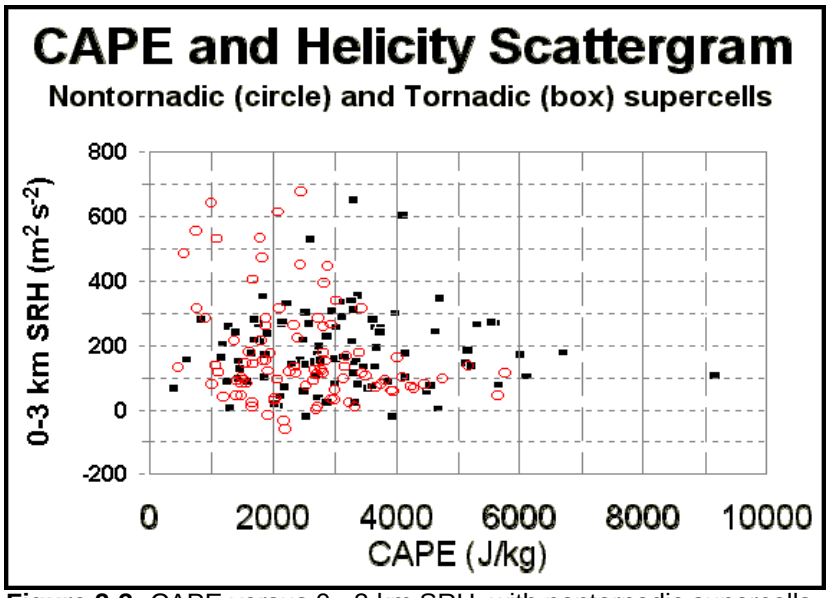

Figure 2-3. CAPE versus 0 - 3 km SRH, with nontornadic supercells as open circles and tornadic as squares (Edwards and Thompson, 2000)

- In low CAPE environments (such as in the cool seasons), stronger shear environments may be sufficient to produce tornadic storms. External forcing mechanisms (such as fronts, upper-level jet streaks, and density boundaries) and the strength of the cap (estimated by CIN) also play a large part in modulating convective initiation, storm structure and resultant storm evolution.

Shear and buoyancy (as well as cold pool strength) also play a role in determining squall line and bow echo strength, but their variations and relationships are not as well established as they are for supercells. Objective 13 includes more information on the relationship of shear and buoyancy on squall line and bow echo strength (Multicell thunderstorms include squall lines and bow echoes).

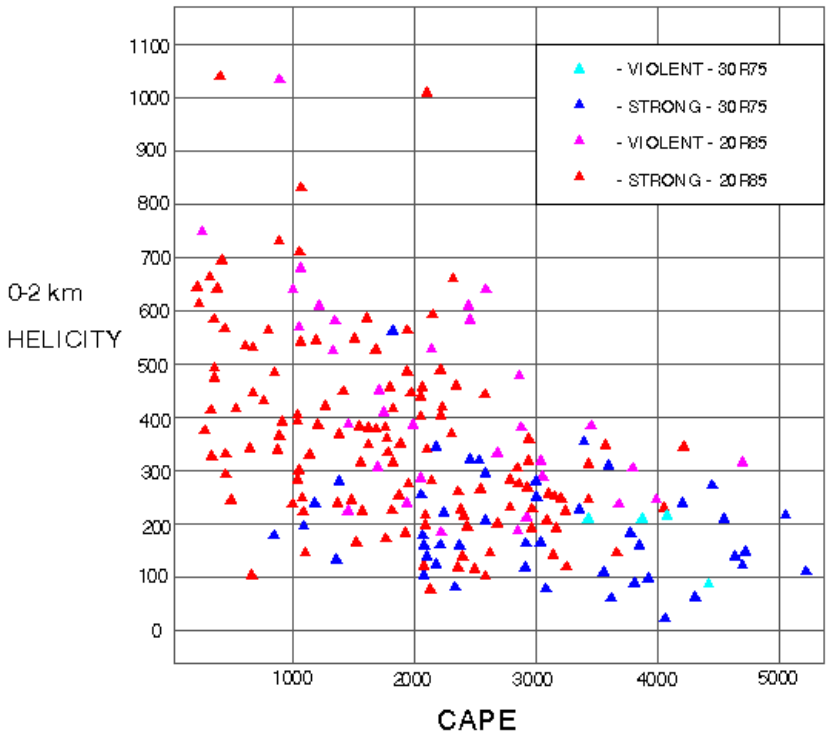

Figure 2-4. CAPE versus 0-2 km SRH for strong and violent tornado cases for two types of storm motion calculations (Johns et al., 1990).

Objective 3

For a given hodograph and magnitude of vertical wind shear, describe the role of midlevel dry air on storm evolution.

Midlevel Dry Air Promotes Stronger Downdrafts

Thunderstorms that form in environments with drier midlevel air (lower wet-bulb potential temperature,Θ_w) will tend to produce stronger evaporatively-cooled downdrafts and wind gusts at the surface (Fawbush and Miller, 1954; Browning and Ludlam,1962; Foster, 1958). The Fawbush and Miller (1954) “Type-I” composite sounding for producing tornadoes exhibited dry, capping air in midlevels originating off the hot, dry high Mexican plateau overlaying moist, boundary layer air from the Gulf Coastal region. Early modeling studies of supercell thunderstorms in the 1980s suggested that greater instability, as measured by CAPE, increased storm downdraft strength (Weisman and Klemp 1982, 1984). In addition, weaker shear,

which implied less entrainment, was found to produce stronger downdrafts.

Effect on Storm Evolution Due to Vertical Placement of Dry Midlevel Air

In a three-dimensional modeling simulation, Gilmore and Wicker (1998) found that midtropospheric dryness helped induce significant differences in low-level supercell storm morphologies and evolutions (Fig. 2-5). For cases with very dry midlevel air (due to smaller vertical wind shear and lower-altitude dry air placements), they found that the resulting low-level outflow moved out faster than the midlevel mesocyclone, which tended to weaken the thunderstorm updraft and the associated mesocyclone. On the other hand, greater midlevel moisture (due to stronger wind shear and/or higher altitude dry air placement), induced a delayed (and weaker) surface outflow which enhanced the updraft. Cases with dry air at higher altitudes were less able to bring their minimum Θ_w air down to the surface due to a reduced evaporative cooling rate aloft and a longer path where mixing between the downdraft and environment would occur. In the greater midlevel moisture cases, the resulting speed of the low-level storm features maintained alignment of the midlevel mesocyclone and thus, increased storm longevity.

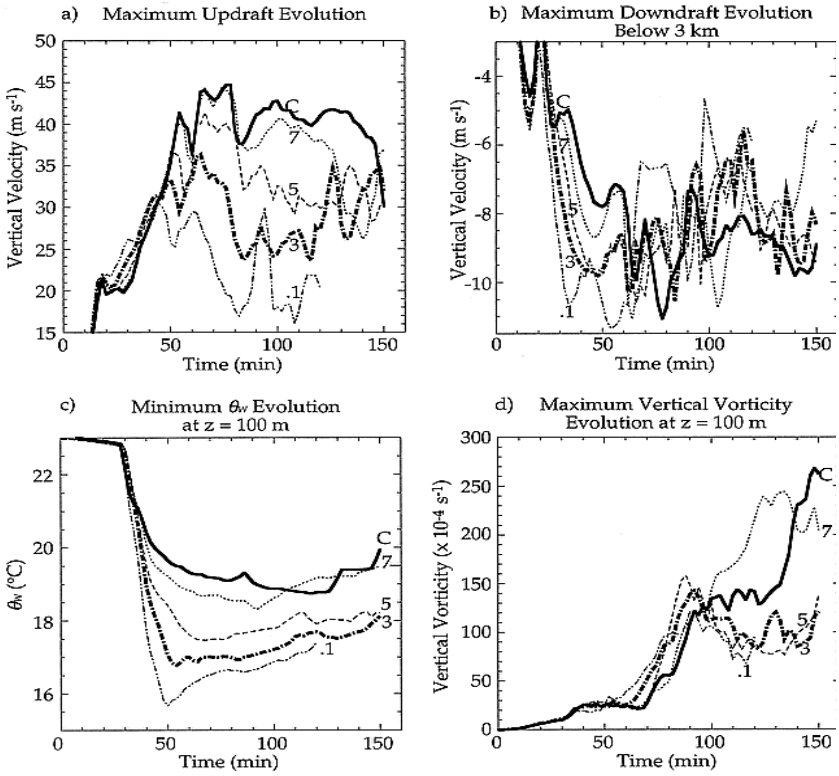

Figure 2-5. Evolutions of a) maximum updraft, b) maximum downdraft below z=3 km, c) minimum Θ_w at z=100 m, and d) maximum vertical vorticity at z=100 m for supercell simulations with driest modified air at z=2.3 km. The value "C" represents the control case while others are represented by their respective water vapor mixing ratios (g/kg) at the height of the driest modified air. Two minute sampling from the model data is plotted. (From Gilmore and Wicker, 1998)

Downdraft Convective Available Potential Energy (DCAPE)

The downdraft potential of the simulated environment from Gilmore and Wicker (1998) was represented by a parameter called DCAPE [Downdraft Convective Potential Convective Energy; Emanuel (1994)]. According to results from Gilmore and Wicker (1998), DCAPE was shown to be a poor indicator of downdraft intensity, or low-level outflow strength, due to parcel theory assumptions. Entrainment of environmental dry air dilutes thunderstorm downdrafts and significantly changes the Θ_W of parcels. This dilution increases with greater vertical wind shear or when downdraft parcels with low Θ_W descend from higher altitudes. As a result,

increases in kinetic energy due to evaporative cooling within the downdraft are much less than predicted.

Dichotomous Effects of Dry Midlevel Air

Numerical cloud model simulations in *A Convective Storms Matrix* showed soundings with similar CAPE and shear but different midlevel relative humidity profiles such that dry midlevel air seemed to weaken the storm system. However, the dry midlevel air did enhance the surface cold pool produced by the rainy air in the downdraft. Thus, in some cases, midlevel dry air, especially when it is associated with steep, midlevel temperature lapse rates, can enhance the strength of multicellular systems like squall lines and bow echoes. The reason for this dichotomous effect is that midlevel dry air can be entrained into both convective updrafts and downdrafts, decreasing potential updraft buoyancy, but increasing potential downdraft negative buoyancy.

Rules of Thumb for Mean Relative Humidity (RH)

Based on operational severe storm forecasting rules, mean Relative Humidity (RH), as indicated from raobs and model soundings as the average RH in the column from near the surface (~1000 mb) to midlevels (~500 mb), is usually greater than 40-45% in severe thunderstorm environments. This empirical rule is a result of synoptic environments supportive of severe weather containing a dry midlevel layer overlying a moist boundary layer. If the environment indicates more saturation through a deep layer (70% mean RH), then, all other factors being equal, storms are more likely to produce heavy rain as opposed to organized severe weather. Thus, as is the case with most other thermodynamic parameters, storm or system evolution is not simply related to a single parameter such as midlevel dry air.

Inverse Relationship Between DCAPE and Mean Winds in Estimating Cold Pool Strength

A recent study (Evans and Doswell, 2001) of derecho environments using proximity soundings suggested that there is an inverse relationship with DCAPE and mean wind (0-6 km). DCAPE was used as an estimate of the potential cold pool strength. When the mean wind and large scale forcing were weak, the potential for strong downdrafts and resulting cold pools played a dominant role in creating strong surface winds. On the other hand, when the mean wind and synoptic forcing were strong, severe surface winds occurred with relatively weak downdrafts and cold pools. Thus, midlevel dry air might not be as important when stronger environmental winds (and shear) are present.

Objective 4

Explain the role of shear depth in controlling the resulting storm structure and evolution.

In numerical modeling simulations, when a 7.5 km-deep shear length capable of producing supercells (Fig. 2-6) is shrunk to a depth of 2.5 km (Fig. 2-7), the shallower shear tends to create intense cold pools which then proceed away from developing supercells thereby cutting off their inflow. These intense cold pools also promote deeper lifting along their leading edges helping to generate more ordinary cells organized in lines and bows (Fig. 2-7).

More discussion on the influences of shear depth and magnitude on storm structure and evolution is presented in later lessons.

.

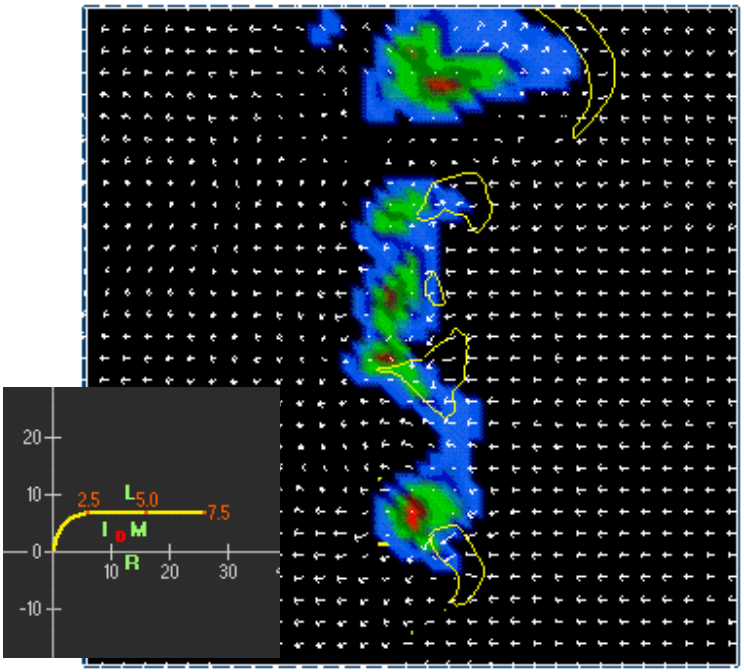

Figure 2-6. Planview map at 4 km above surface of a model simulation of convection three hours after initiation using the hodograph with 30 m/s of shear over 7.5 km. Colored regions represent vertical velocity while thin yellow isohyets are vertical vorticity. The white vectors are system-relative winds. From the *Convective Storm Matrix* (COMET 1995).

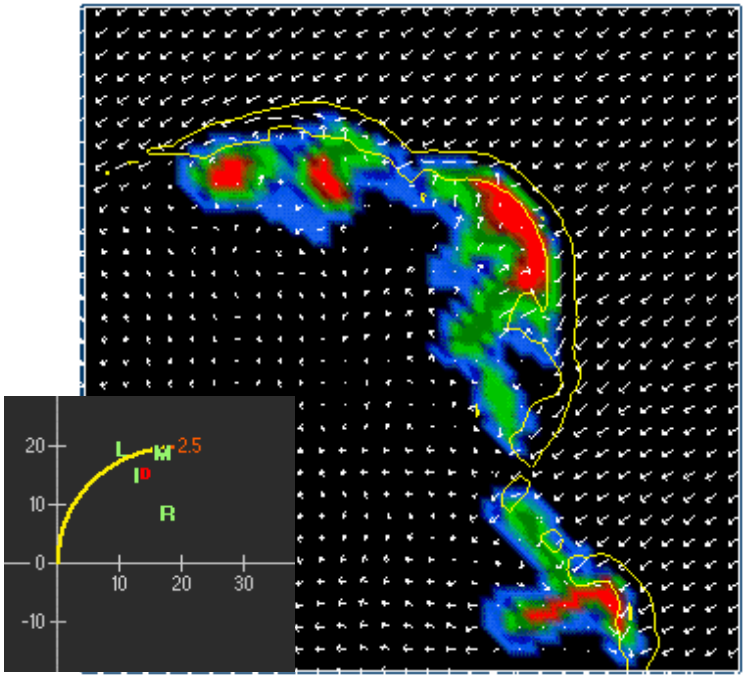

Figure 2-7. As in figure 6 except now there is 30 m/s of shear over 2.5 km. From *The Convective Storm Matrix* (COMET 1995).

Objective 5

Explain the role of hodograph curvature in controlling resulting storm structure and evolution for strongly sheared environments.

Both straight and curved hodographs produce equally strong supercells given enough shear. However, straight hodographs allow both the right (cyclonic) and left (anticyclonic) moving supercells to be equally strong. Clockwise (counterclockwise) turning hodographs favor the right-moving (left-moving) supercell and weakens the left-moving (right-moving) member. As an example, note the mirror image cyclonic and anticyclonic supercells in Figure 2-8 in an environment characterized by unidirectional shear (straight hodograph example). Conversely, applying the curved hodograph with the same shear magnitude, the cyclonic supercell dominates and the anticyclonic supercell is almost

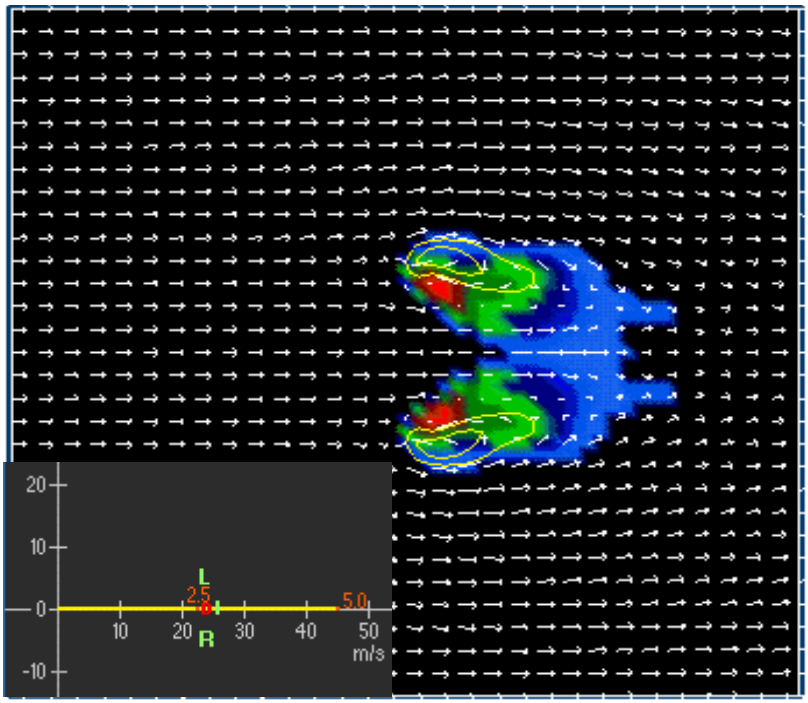

Figure 2-8. Model simulation of updraft strength (shaded colors) and vorticity (yellow contours) at 4.6 km above surface and 1.5 hours after initiation for the straight hodograph shown in the inset. The hodograph has 46 m/s of shear over five kilometers. From *The Convective Storm Matrix* (COMET 1995).

gone (Fig. 2-9). Review *A Convective Storm Matrix* (COMET, 1995) to explore other examples of straight and curved hodographs with varying shear magnitudes.

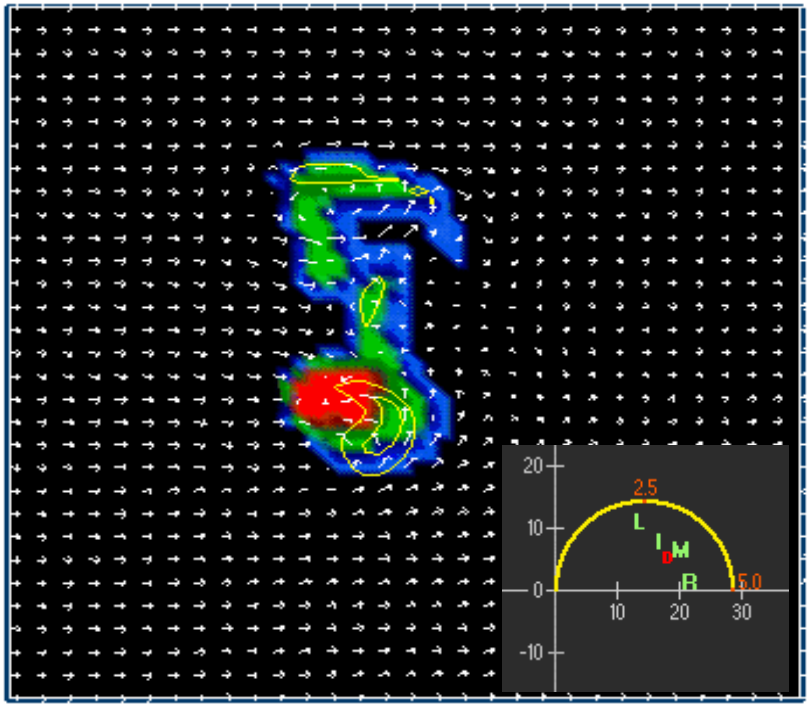

Figure 2-9. Similar to Figure 2-8, except for a curved hodograph with similar shear. From *The Convective Storm Matrix* (COMET, 1995)

Another way to analyze the differences between straight and curved hodographs is from a streamwise vorticity perspective (Davies-Jones, 1984). An updraft moving with the mean wind in a unidirectional shear environment (straight hodograph) tilts only crosswise vorticity. To create a rotating updraft, it is necessary to tilt streamwise vorticity. The updraft must move off the hodograph before being able to tilt streamwise vorticity. An updraft moving with the mean wind in a clockwise-turning curved hodograph is able to tilt streamwise vorticity without even having to move away from the mean wind.

Lesson 3: Definitions, Strengths, and Limitations of Environmental Parameters

Objectives 6 - 8

Objective 6. Identify definitions, strengths, and limitations of some of the most operationally relevant kinematic and thermodynamic parameters for forecasting convective storm type.

Objective 7. Identify the physical process associated with the convective storm parameters listed in Objective 6.

Objective 8. Describe the basic relationships between shear and instability in forecasting severe storm type.

Buoyancy

Several thermodynamic and kinematic parameters have been developed to assess the vertical distribution of buoyancy for the purpose of evaluating convective severe weather potential. Many thermodynamic stability indices such as Lifted Index (LI) or Showalter Index (SI) can easily be computed via sounding analysis from a Skew-T Log-P Diagram (See RTM-230).

CAPE

The best thermodynamic parameter to assess buoyancy is CAPE, defined as Convective Available Potential Energy. CAPE is a cumulative measure of the positive buoyant energy (in J/kg) a rising parcel of air would have once the parcel passes its Level of Free Convection (LFC) all the way to its Equilibrium Level (EL); See RTM-230 for the definition and graphical representation of CAPE. CAPE is not a measure of instability in the sense of the LI or SI, which use a temperature difference between rising parcels and the environment at a single level, but rather a vertically integrated quantity. Thus, there is not a one-to-one

relationship between CAPE and instability. CAPE depends on instability and the depth of integration. There are often big differences between model-derived computations of CAPE values and CAPE values derived from observed sounding data. These differences result from several factors, including:

Model CAPE Discrepancies

1. Assimilation and initialization processes used in the models. These processes incorporate more data than raobs (including first guess fields), such that model soundings at initialization are not exact duplicates of actual soundings.

2. The methodology that is used to determine from where the parcel is lifted. The method of lifting the parcel with the most unstable characteristics in the lowest 300 mb (AGL) often produces the most reliable estimates of CAPE in all situations (SPC, private communication).

Importance of CAPE Density, 0-3 km CAPE

CAPE is very sensitive to both the magnitude of buoyancy and the depth of the integration. Modeling work by Wicker and Cantrell (1996) examining mini-supercells found that the coupling of low-level shear and small values of low-level CAPE (i.e., CAPE located in the lowest 1-3 km) appeared to be more important for the development of rotational characteristics within these storms than were larger values of CAPE through a deeper layer. Some of the mini-supercell CAPE values were as low as 600 J/kg in simulations which produced significant low-level accelerations and vertical velocities. Other research such as McCaul and Weisman (1996) and Johns and Doswell (1992) have also noted that a large fraction of supercell cases nationwide arise in situations where CAPE values are less than 1500 J/kg (likely mini-supercells or low-topped events). Grant (1995) found that the average CAPE as deduced from proximity

soundings in elevated severe thunderstorms was approximately 700 J/kg. Blanchard (1998) suggested that it is possible for environments to have similar CAPE values but different degrees of instability. The vertical distribution of CAPE, whether the CAPE area is “tall and thin” or “short and wide”, should be considered when assessing the convective potential of a sounding. Normalized CAPE (NCAPE), introduced by Blanchard (1998), may provide forecasters with a better indication of instability in environments in which the depth of free convection is shallow (low-topped mini-supercells or tornadoes associated with landfalling tropical storms).

Convective Inhibition (CIN)

To effectively evaluate the effects of buoyancy in forecasting severe weather type, one must also assess Convective Inhibition (CIN). CIN is a measure of the “negative area” on a sounding between the surface and the LFC. CIN is a measure (in J/kg) of the capping-intensity of the atmosphere and assesses the ability of the vertical temperature profile to suppress surface-based convection. In most cases, when an air parcel moves upward away from the earth's surface, it will be cooler than the surrounding environment until it moves above the Level of Free Convection (LFC). This negative buoyancy implies that surface-based convection must be forced upward beyond the LFC before an updraft will be sustained. CIN measures the negative buoyancy working against this rising parcel. In situations of elevated convection, the forcing mechanism acts to lift parcels above the stable capping layer and thus, does not necessarily have to overcome all the negative buoyancy. In those cases, a strong cap (large CIN) might be favorable for sustaining the convection given sustained synoptic or mesoscale forcing and sufficient instability existing above the stable surface layer.

Lifting Condensation Level

The Lifting Condensation Level (LCL) is the height at which a parcel becomes saturated when lifted dry adiabatically (See RTM-230). It is related to the amount of low-level relative humidity which would affect cooling through evaporation of rain in the downdraft portion of a storm. The higher the LCL is in the storm environment, the drier the boundary layer will be. Rasmussen and Blanchard (1998) showed that LCLs in tornadic supercell (TOR) soundings were significantly lower than that for nontornadic supercells (SUP) and in nonsupercell storms (ORD). Half of their TOR soundings had LCLs below 800 m, while half of their SUP soundings had LCLs above 1200 m. Substantial variations undoubtedly occur on small time and space scales with LCLs, so sampling with network soundings may not be representative. Actual LCL heights near tornadic supercells may be considerably lower than those documented in research.

Shear

Several parameters are used to estimate vertical shear, which, along with buoyant energy, strongly influences what type of convective storm may develop. Forecasters typically analyze hodographs (both hodograph curvature and overall length) in the lower troposphere to assess vertical wind shear (See RTM-230 and the Background Section of the *Convective Storm Matrix* for a good explanation of hodographs). Vertical wind shear, as you recall from Objective 1, is the most important factor for storm organization. Surface-to-6 km (AGL) shear has been used extensively in research and operations for evaluating environments that support supercell storm processes. Hodograph length, which measures the total magnitude and depth of vertical wind shear, is easily calculated by adding up the wind vectors along the hodograph through a certain layer. This total value (in m/s) can be used to estimate if the dynamics of

internal storm rotation in supercells are likely if thunderstorms develop. Typically, the lower bound threshold of hodograph length for supercells (as derived from observed and model soundings on the synoptic scale) is around 20 m/s (from SPC communication).

Minimum Shear for Supercells

In numerical modeling simulations (Weisman, 1992, 1993) environments that had hodograph lengths greater than 20 m/s (with CAPE values of at least 2000 J/kg) over the lowest 2-3 km AGL were often associated with very long-lived, multiple storm systems. However, in analyzing proximity soundings along the path of mature derechos, Evans and Doswell (2001) found much lower values of 0-2 km shear were common, with three-fourths of the cases containing shear magnitudes less than 16 m/s, and values ranging from near 3 to 30 m/s. These shear values were found in cases typically associated with 0-6 km shear vector magnitudes less than 20 m/s, weak forcing, and high values of CAPE.

Shear in Tornadic and Nontornadic Supercells

From analyzing over 6000 proximity soundings, Rasmussen and Blanchard (1998) established a baseline climatology of several severe storm kinematic parameters, such as Boundary-Layer-(BL)-to-6 km shear vector, mean shear, Storm-Relative Helicity, and storm-relative upper-tropospheric wind speed. All of these parameters showed some value in differentiating between supercell and non-supercell environments. However, BL-to-6 km shear had no utility for distinguishing between supercells which produced significant tornadoes and those which only produced large hail. On the other hand, Storm-Relative Helicity (SRH) and boundary mean shear, which was computed as the length of the hodograph divided by the depth of the layer measured (4 km in their studies), were

better able to distinguish between supercells that produced significant tornadoes and those that only produced large hail. In the study of kinematic parameters, SRH showed the best discrimination ability between storm type categories (Fig. 3-1), suggesting that the streamwise component of horizontal vorticity is the component that dominates in the production of rotating updrafts in supercells.

Storm Relative Helicity (SRH)

SRH is proportional to both streamwise vorticity and storm-relative winds and takes into account storm motion. The equation for SRH, as defined by Davies-Jones et al. (1990), is

$$SRH = \int_0^h (V - C) \bullet \omega dz \qquad (3\text{-}1)$$

where V is the horizontal velocity (ground-relative vector wind), C is the storm motion, and ω is the horizontal vorticity vector. The integration is over the inflow layer of the storm from 0 km (the ground) to some depth h (typically 1 to 3 km).

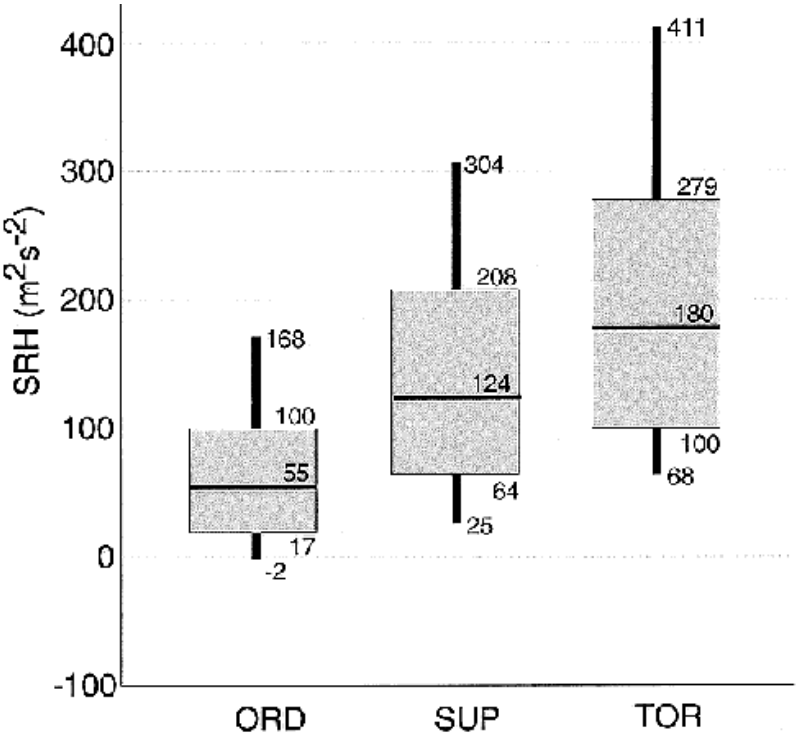

Figure 3-1. Box and whiskers graph of Storm-Relative Helicity (0-3 km) for soundings associated with supercells with significant tornadoes (TOR; right), supercells without significant tornadoes (SUP; middle), and nonsupercell thunderstorms (ORD; left). Gray boxes denote the 25th to 75th percentiles, with the heavy horizontal bar at the median value. Thin vertical lines (whiskers) extend to the 10th and 90th percentiles (Rasmussen and Blanchard, 1998).

Correlations in SRH and Tornado Intensity

Johns et al. (1990) and Davies-Jones et al. (1990), using observed storm motions in calculations of SRH, indicated correlations between increasing SRH values and tornado intensity. The observed 0-2 km mean SRH magnitude for strong (F2/F3 tornadoes) was about 360 m^2s^{-2}, while the mean SRH for their violent (F4/F5) category tornadoes was about 450 m^2s^{-2}.

Can You Predict Maximum Tornado Intensity From SRH?

Kerr and Darkow (1996) examined SRH values for 184 tornado proximity soundings. The table below (Table 3-1 below) shows the mean SRH values for the corresponding F-scale intensities. Their study

contained no F5 tornado proximity soundings. The mean SRH for the entire data set was 142 m^2s^{-2}.

Table 3-1: SRH vs. F-scale (from Kerr and Darkow, 1996)

F-scale	F0	F1	F2	F3	F4
Helicity value m^2s^{-2}	66	140	196	226	249

They concluded that by examining regions where CAPE values were positive and 0-3 km SRH values were greater than 100 m^2s^{-2}, one could generally identify areas where supercell thunderstorms were possible if convection developed.

SRH is a Better Supercell Forecasting Tool

These types of studies suggest that SRH may have some predictive value as a tornado forecast tool. However, later studies have shown that it is a much better tool for estimating supercell potential as opposed to tornado potential. Two problems for using SRH as a forecast tool are that an estimate of storm motion is required and the depth for computing SRH is critical. Deviant right motion is often observed, but the speed of storms vary considerably depending on external factors. This is why using hodograph length as a shear parameter can be an advantage over SRH in providing an estimate of rotation potential before storms develop.

Depth of SRH to be Used

In the past, the depth chosen for calculating SRH was usually 3 km. Recent and ongoing studies (e.g., Rasmussen, 2001) have found that the near ground (0-1 km AGL) layer may have critical implications to tornado potential in supercells (Fig. 3-2) and actually have better discrimination ability than 0-3 km SRH.

Thus, it is important to conclude from all of these studies that large SRH values (at any level) does

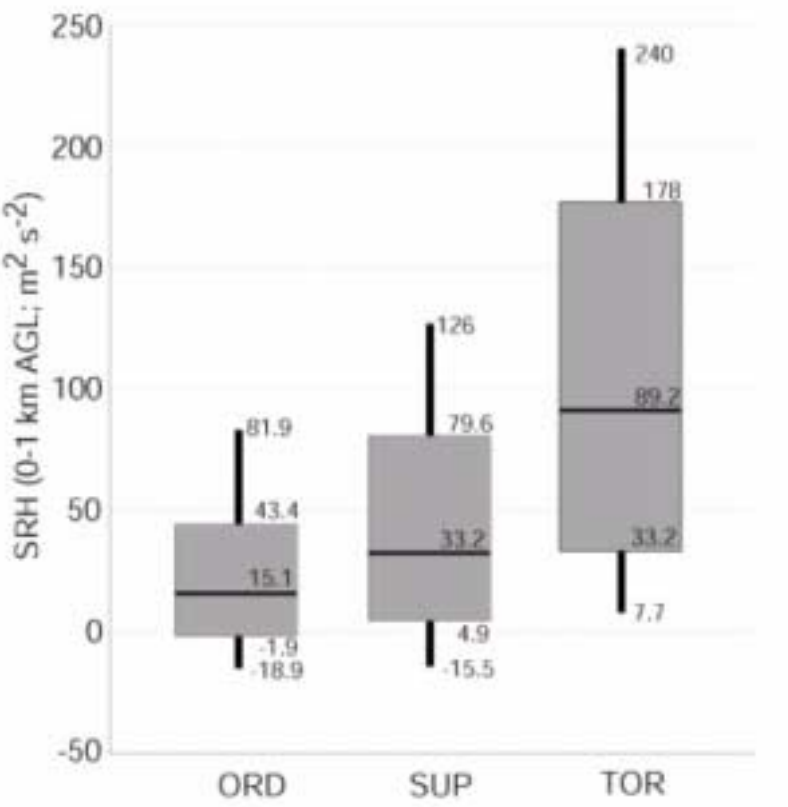

Figure 3-2. Similar to Figure 3-1 except for 0-1 km AGL SRH for soundings associated with supercells with significant tornadoes. (From Rasmussen, personal communication)

not imply that a particular sounding will be associated with a significant tornado. In the Rasmussen and Blanchard (1998) study, almost 25% of their nonsupercell soundings (600 soundings) had SRH values between 100 and 168 m^2s^{-2}. That amount is more than the total number of soundings in both of the supercell categories. Since forecast storm motion is used in the computations of SRH, it is important to re-analyze your local estimates of SRH once observed storm motions are known.

Midlevel Flow in Tornadic and Nontornadic Storms

The role of midlevel shear has also been investigated in the prediction of storm type. Specifically, the character of the midlevel storm-relative flow has been shown to influence the production of low-level mesocyclones and the potential for storms to produce significant tornadoes (Thompson, 1998).

Thompson found that supercells were more likely to produce tornadoes when the midlevel (estimated at 500 mb) storm-relative winds were greater than 8-10 m/s.

Shear and Buoyancy Combinations

BRN

Mean shear, as well as SRH, becomes a much stronger predictor of supercells and tornadoes when paired with CAPE. The Bulk Richardson Number (BRN) has been used as a supercell predictor ever since it was investigated using numerical simulations (Weisman and Klemp, 1982).

BRN is a rough measure of the buoyancy to shear ratio.

$$BRN = CAPE / ½ (U^2), \quad (3\text{-}2)$$

where CAPE is Convective Available Potential Energy and U is the bulk shear, determined by subtracting the density-weighted mean wind vector in the lowest half-kilometer layer from the density-weighted mean wind vector in the lowest six-kilometer layer.

BRN vs. BRN Shear

Weisman and Klemp (1982, 1984) determined that environments with BRN < 50 favored the development of supercells, while BRN > 35 favored multicells. The overlap area (35 > BRN > 50) suggested that both supercells and multicells were possible at the same time. Operational viability of this parameter is questionable because of the wide range of CAPE values typically observed in environments which produce tornadoes. For very large values of CAPE (> 4000 J/kg), the BRN is dominated by the CAPE such that BRN is large

regardless of the values in the denominator (known as BRN shear; Stensrud et al., 1997).

Other BRN Limitations

Moreover, Rasmussen and Blanchard (1998) found that even though 75% of their (SUP) supercell soundings had BRN values < 17, over 50% of the ORD (ordinary thunderstorm) soundings had those values as well. In addition, another limitation is that BRN does not account for detailed aspects of the wind profile, particularly low-level curvature. Johns et al. (1990) examined the mean shear and buoyancy values for 242 strong-to-violent mesocyclone-induced tornadoes. From proximity soundings, their study showed 15% of the tornado events had CAPE values less than or equal to 1000 J/kg, with 47% of the events having BRN values less than 8. One explanation that was offered for the low BRN values is that in low-buoyancy environments, shear-induced pressure forces, related at least in part to the low-level curvature shear, can be the dominant factor in controlling updraft strength. Therefore, it appears likely that in many situations where the BRN value is a very low value and supercells do occur, that the low-level curvature shear plays a crucial role in helping to sustain the rotating updrafts.

BRN Shear Values for Nontornadic and Tornadic Supercells

The denominator of BRN (½ (U^2)) was shown by Stensrud et al. (1997) to be a surrogate for storm-relative midlevel flow, citing the advantage that BRN shear is independent of storm motion. Utilizing MM4 mesoscale model output in their study of selected severe weather cases, they found that BRN shear values of 40-100 m^2/s^2 indicated a significant possibility of tornadic supercell storms, whereas values less than 40 m^2/s^2 were associated with storms dominated by outflow (e.g., bow echoes).

Energy Helicity Index (EHI)

The Energy-Helicity Index (EHI; Hart and Korotky, 1991; Davies 1993) is defined as

$$EHI = (CAPE)\,(SRH) / 1.6 \times 10^5 \qquad (3\text{-}3)$$

This index is used operationally for supercell and tornado forecasting, with values > 1.0 indicating a potential for supercells, and values > 2.0 indicating a high probability of supercells. As with BRN, EHI has some value in discriminating between supercells that produce tornadoes and those that do not (Fig. 3-3). The main forecasting application of using EHI is that the likelihood of significant tornadoes increases with increasing EHI.

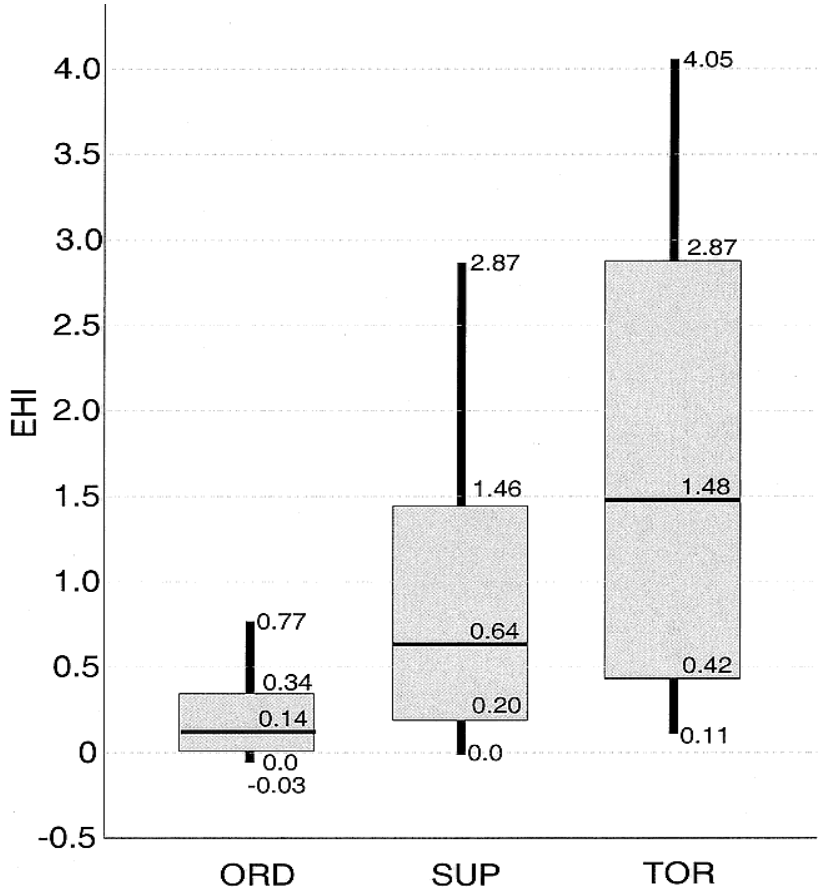

Figure 3-3. As in Figure 3-1, except for Energy Helicity Index (EHI). From Rasmussen and Blanchard (1998).

Vorticity Generation Parameter (VGP)

The Vorticity Generation Parameter (VGP) is derived from an examination of the parameter space investigated in Rasmussen and Wilhemson

(1983) and the physical concept of tilting of horizontal vorticity (to vertical vorticity). The equation used by Rasmussen and Blanchard (1998) is

$$VGP = [S(CAPE)^{½}], \qquad (3\text{-}4)$$

where S was the mean shear (hodograph length divided by depth). Mean shear was assumed to be proportional to the horizontal vorticity vector and $CAPE^{½}$ proportional to the vertical component of velocity. So VGP was roughly proportional to the rate of tilting of horizontal vorticity to vertical vorticity. Similar to EHI, VGP has been shown to significantly discriminate between supercells and nonsupercells, but is not as good as low-level shear (SRH) paired with CAPE at distinguishing between storms with significant tornadoes.

Summary

The combination of CAPE and shear in parameters such as EHI or VGP improves the use of soundings in discriminating between supercells with significant tornadoes, supercells with no tornadoes, and ordinary thunderstorms. Evaluating shear and CAPE together helps to provide ranges for potential storm evolutions. For forecasting storm type, one must first assess the synoptic-scale environment to analyze regions of low-level moisture, instability and lift. Proximity soundings can tell us a lot about the potential for a specific type of severe weather such as tornadoes, large hail, or damaging wind. However, changes in the mesoscale environment often strongly influence the large scale conditions and dictate the eventual severe weather mode. Often, multiple convective modes exist simultaneously making a priori assessment of a preferred storm type quite difficult.

One must be aware that there is a high false alarm rate for any parameter value derived from any given sounding. The distributions in the parameter spaces discussed in Rasmussen and Blanchard (1998) and Johns et al. (1990) bear this fact out. Limitations in sampling the actual storm environment also contribute to considerable estimations to reality. Combinations of several parameters, indicating not only the updraft-based aspects of the storm but also the downdraft aspects, will likely provide the best forecast of eventual storm type.

Lesson 4: Propagation and Evolution of Convection

Objective 9

Describe the physical mechanisms that determine the motion for ordinary cells.

Single Cell Storms

Single cell storms in the absence of shear move with the flow at any level (which is not surprising since the flow at any one level is the same as any other level). Adding vertical wind shear complicates predicting single storm motion since an updraft experiences a range of flows depending on the storm's depth and the magnitude of the shear. However, early studies such as the "Thunderstorm Project" have found a good relationship between a mean steering-layer wind and thunderstorm motion (Byers and Braham, 1949). Most schemes for estimating convective steering-layer flow calculate the mean 0-6 km AGL wind.

0-6 km Mean Wind

Since air density increases exponentially toward the ground, a common mean wind calculation is weighted by density giving more influence to the influence of low-level flow to steering thunderstorms. Using the raw 0-6 km mean wind or the 0-6 km density-weighted mean wind provides a relatively accurate method for estimating ordinary thunderstorm motion for most cases. If the averaging utilized a deeper layer, say 0-12 km, then weighting the average by density becomes more important to producing accurate results.

Cautions About Using 0-6 km Mean Winds

There are cautions about using a 0-6 km mean wind for estimating ordinary thunderstorm motion. Low- (high-) topped thunderstorm motion may be influenced better by a shallower (deeper) mean wind. For example, Wilson and Megenhardt (1997) found a reasonable steering layer flow for summertime Florida thunderstorms was the 2-4 km layer. However, for the typically deeper thun-

derstorms on Tiwi Island (near Darwin, Australia), the same layer mean wind calculation proved less accurate in estimating thunderstorm motion (Wilson et al., 2001).

Objective 10

Describe the physical mechanisms that determine the motion for supercell convection.

a. How does unidirectional shear affect supercell propagation?

b. How does directional shear affect supercell propagation?

Straight Hodograph Dynamic Processes

This concept is explained in the COMET CD-ROM module, *Anticipating Storm Structure and Evolution,* under the section called *"Straight Hodograph Dynamic Processes"*. Horizontal shear acts upon the updraft of a storm, forcing the storm to move away from the convective steering layer flow. Remember that horizontal shear results in horizontal vorticity, which the updraft then reorients to generate counter-rotating vortices on either side of the updraft (Figure 4-1).

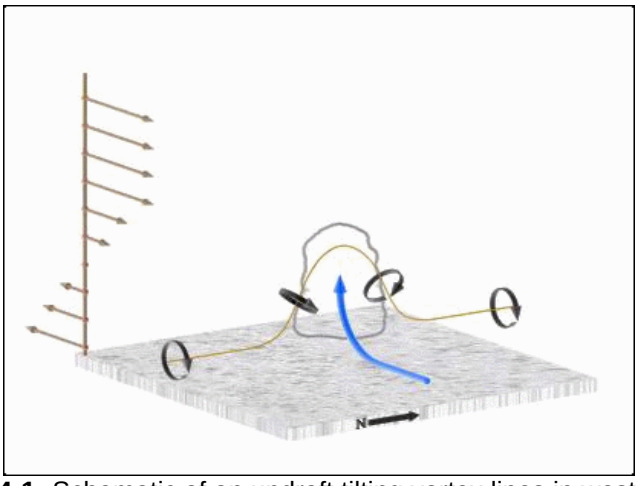

Figure 4-1. Schematic of an updraft tilting vortex lines in westerly shear. Adapted from COMET (1996)

Dynamically Driven Low Pressure in Each Vortex

Within the center of these vortices, a dynamically driven area of low pressure develops in each vor-

tex center at midlevels (Fig. 4-2). Each low acts to promote new updrafts through the center of each vortex, in effect widening the updraft in an axis perpendicular to the shear vector.

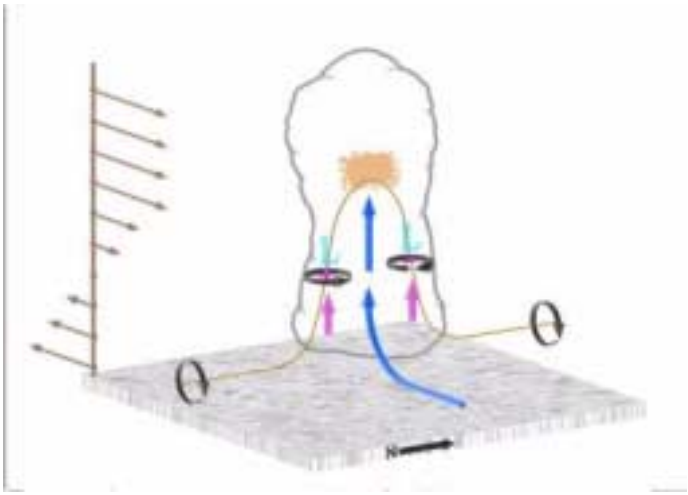

Figure 4-2. Schematic of dynamically driven low pressure forming on either side of an updraft. From COMET (1996).

The greatest tilting occurs right and left of the shear vector. Precipitation developing in the middle of the widening updraft acts to develop a downdraft which, in turn, helps to split the widening updraft into two parts (Fig. 4-3). The cyclonically (anticyclonically) rotating member moves to the right (left) of the shear vector. Since both the cyclonic and anticyclonic updrafts experience similar upward dynamic pressure forcing, they are equally strong supercells.

The Cyclonically (Anticyclonically) Rotating Member Moves to the Right (Left) of the Shear Vector.

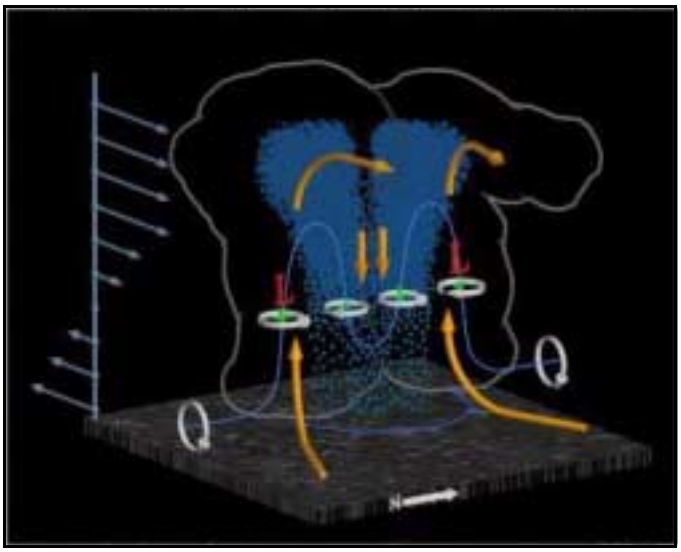

Figure 4-3. Schematic of downdraft formation and subsequent retilting of vortex lines downward. Adapted from COMET (1996).

Plotting Supercell Motion

To plot the location of the right- and left-moving members of the supercell pair on a hodograph, draw a line perpendicular to the 0-6 km shear vector that passes through the 0-6 km mean wind. The right- (left-) moving member will be located on the line 3-8 m/s to the right (left) of the wind shear vector along your line. An example of a linear hodograph (Figure 4-4) shows where to place the right- and left-moving pairs of a splitting storm. The COMET module contains more examples of estimating deviant storm motion from unidirectional hodographs.

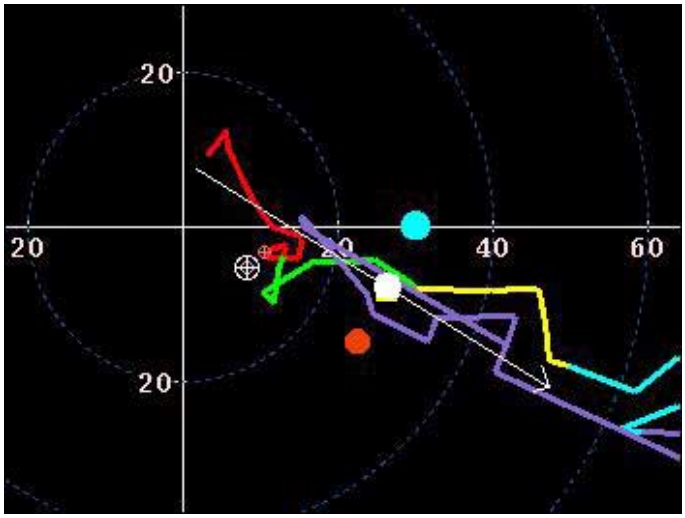

Figure 4-4. Motion of the cyclonic and anticyclonic rotating supercell plotted as a red and cyan dot respectively on a hodograph. The thin white arrow represents the 0-6 km shear vector and the white dot is the 0-6 km mean wind.

Curved Hodographs

While the same processes that promote deviant motion in unidirectional hodographs will work in curved hodographs, the interaction of the changing shear vector with height will result in additional processes that promotes growth on only one flank of an updraft. This additional process is related to the same processes that force an updraft to tilt in the presence of vertical shear. On the upshear side of an updraft, high dynamic pressure forms as a result of partial flow blockage, while low pressure forms on the other side (Fig. 4-5) forcing the updraft to tilt.

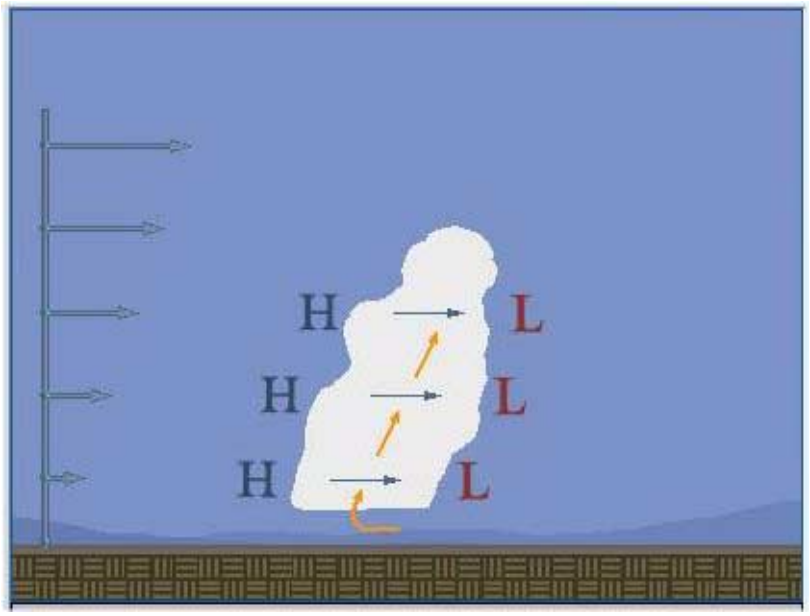

Figure 4-5. A schematic of updraft tilting through differential dynamic pressure induced by unidirectional shear. Adapted from COMET (1996).

Changing Shear Creates Upward (Downward) Gradient on Upshear (Downshear) Side

When the shear profile changes with height (Fig. 4-6), so do the locations of the dynamic pressure maxima and minima. For example, in an environment with clockwise turning shear with height, the lower parts of an updraft will experience relative high (low) pressure on the upshear (downshear) side. In the example hodograph (Figure 4-6), the relative high is on the south side of the updraft at low levels (Figure 4-7). At higher levels, the shear

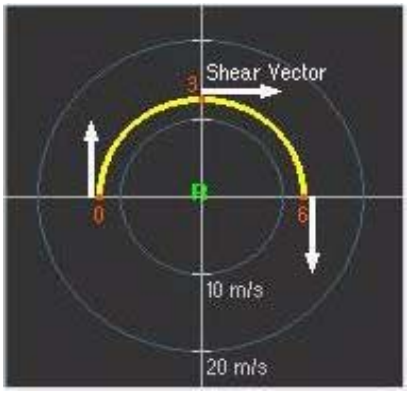

Figure 4-6. A schematic 180° curved hodograph resulting in the dynamic pressure perturbation structure shown in Figure 4-7.

vector pointing south would produce a relative low on the south side of the updraft. The result is an

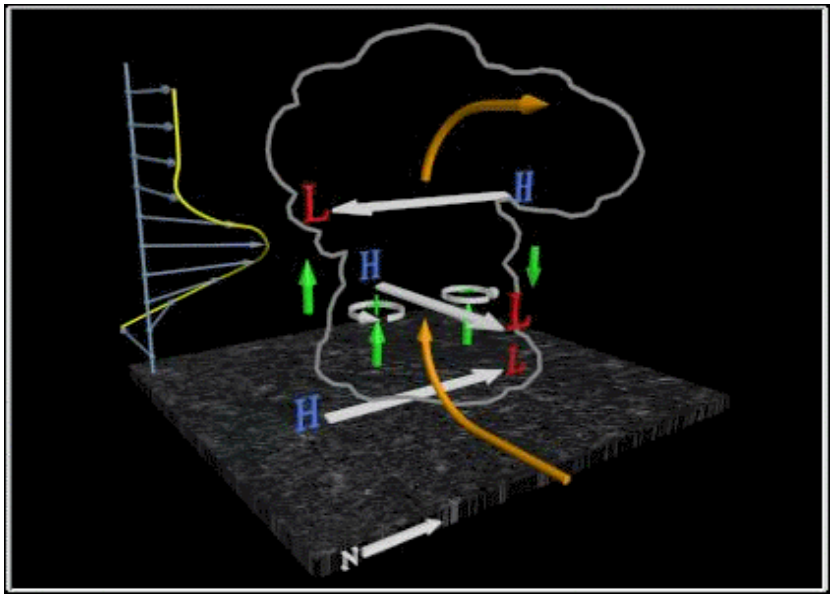

Figure 4-7. A schematic storm structure resulting from the hodograph in figure 7. The labels, L and H, represent dynamic perturbation pressure minima and maxima respectively. The green arrows represent vertical motions forced by the vertical perturbation pressure gradients. Adapted from COMET (1996).

upward directed pressure gradient force that causes new updraft development and therefore storm propagation to the south of its original motion. Meanwhile, the north side of the updraft would experience a downward directed dynamic pressure gradient force weakening, or even destroying, the side of the updraft containing the anticyclonic member of the rotational couplet. This is why a left-moving storm given the hodograph in Figure 4-6, would be suppressed.

Estimating the Amount of Deviant Motion

Estimating the amount of deviant motion in a curved hodograph situation is a bit more problematic, primarly due to the difficulty in estimating the mean steering layer wind. In Figure 4-6, the mean 0-6 km wind is zero. The shear vector is estimated from subtracting the highest level wind from the lowest layer which turns out to be westerly. Thus the cyclonic supercell motion would deviate from

the zero mean wind at 90° to the right of the shear by anywhere from 3-8 m/s. Currently there is no method to determine a priori the speed of the deviant motion, only the direction.

Other Propagation Forces

Forcing mechanisms, beyond those of shear interacting with updrafts, may force supercell motion to deviate more or less than theory dictates. For example, high-precipitation (HP) supercell motion may be influenced significantly by cold pool interactions with the environment. Supercells may also tend to travel along boundaries if the steering layer flow is weak enough to allow the boundary to modulate the direction of supercell propagation.

Objective 11

Describe ways to estimate supercell motion from a hodograph.

Two parameters are needed to estimate supercell motion: 0-6 km shear and a convective steering layer wind. Recall from our discussion in Objective 10 that the presence of shear forces an updraft to split resulting in a cyclonic (anticyclonic) updraft which begin to move deviantly from the steering layer flow. The “deviant” component to the total supercell motion vector is perpendicular to the 0-6 km shear vector by anywhere from 3-8 m/s. The cyclonic (anticyclonic) members of the original storm split move to the right (left) of the shear vector and not the steering layer flow.

The Old Supercell Motion Method

In the past, forecasters often based supercell motion on the 30R75 (Maddox, 1976) or 20R85 (Davies and Johns, 1993) rules. The 30R75 rule estimates the cyclonically rotating supercell motion by adding 30° to the right of the 0-6 km steering layer flow direction and 75% of the speed. The 20R85 rule was an adjustment for those supercells embedded in very strong flow. Unfortu-

nately, these estimations are non-physically based and only apply in the Northern Hemisphere with the typical counterclockwise turning hodographs. The AWIPS skew-T program still uses this technique to estimate SRH.

The Internal Dynamics (ID) Method

Bunkers et al. (2000) developed a better method called the ID method (Internal Dynamics), which uses the mechanisms by which updraft and shear interact to cause deviant motion. This method can be used to calculate storm motion for both the cyclonically and anticyclonically rotating supercells resulting from a storm split. The ID method is Galilean invariant allowing for its use in atypical hodographs (i.e., westerly shear with northerly mean winds). To estimate supercell motion using the ID method, the following steps work well:

a. Plot the 0-6 km non-pressure-weighted mean wind. An example in Figure 4-8 shows the mean wind as a red dot.

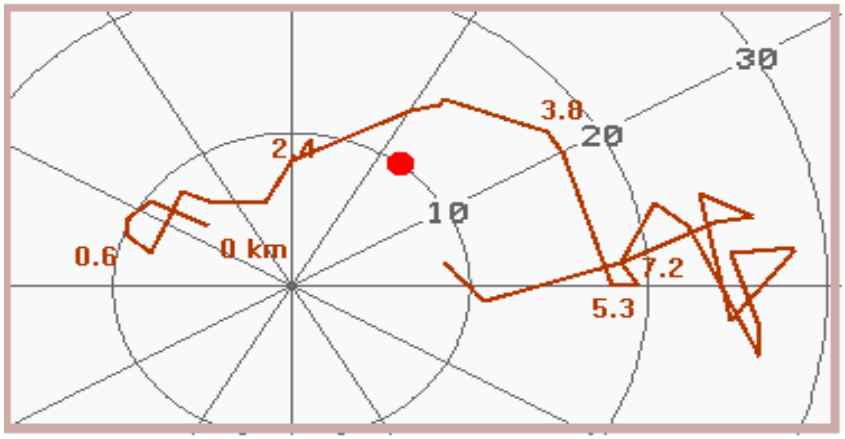

Figure 4-8. A sample hodograph with the 0-6 km mean wind plotted as a red dot. Each ring represents 10 m/s.

b. Draw the shear vector from the mean wind in the lowest 0.5 km to the mean wind from 5.5 - 6 km (Fig. 4-9).

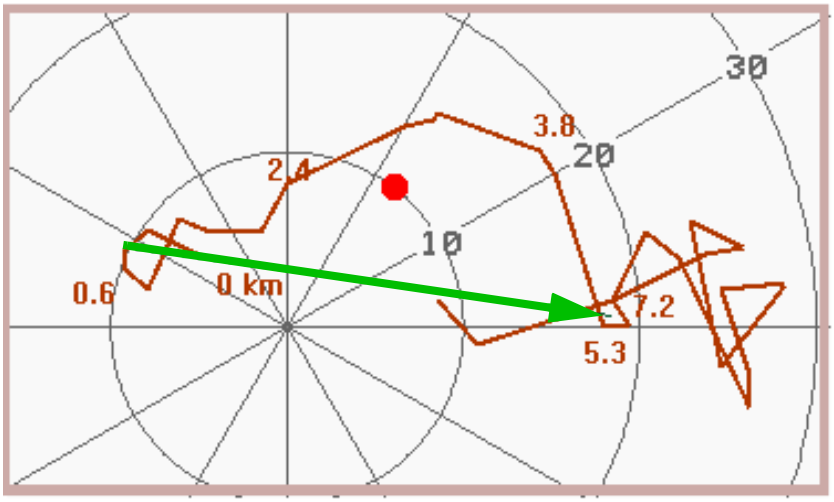

Figure 4-9. Same as Figure 4-8 except the 0-6 km shear vector is added as a green arrow.

c. Draw a line orthogonal to the shear while passing through the mean wind (Fig. 4-10). Note that the shear vector can be placed anywhere on the hodograph as long as it retains the same direction and magnitude.

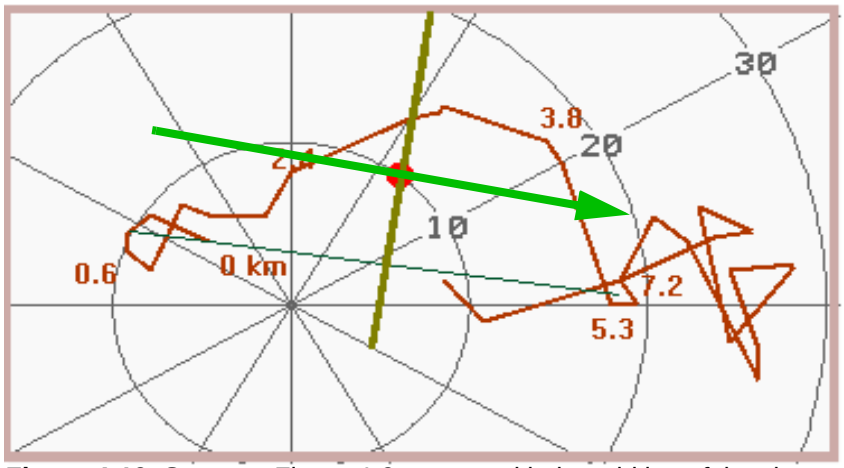

Figure 4-10. Same as Figure 4-9, except with the addtion of the shear-normal line passing through the 0-6 km mean wind (red dot).

d. The right (left) moving supercell is drawn 7.5 m/s to the right (left) of the shear vector where shear vector intersects the shear-orthogonal line at the 0-6 km mean wind.

Note that the storm motion remains on the shear-orthogonal line (Fig. 4-11).

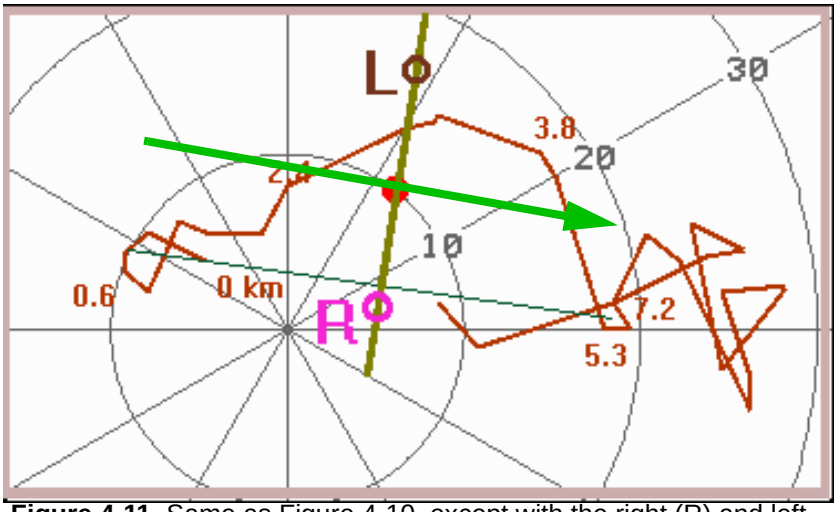

Figure 4-11. Same as Figure 4-10, except with the right (R) and left (L) moving supercells added.

Magnitude of Deviant Motion and Other Issues

Although the ID method is physically-based, there still exists uncertain knowledge on what the deviant motion vector should be. Currently, the 7.5 m/s value is chosen as the most representative value for a large population of observed supercells. Until more is known about how to modulate the deviant motion vector in a physically-based way, there will be differences between observed and predicted supercell motions. It is known that supercells may preferentially propagate along boundaries or other sources of updraft forcing resulting in a motion vector different than that predicted by the ID method. Additional errors may result between observations and predictions because of errors in our analysis of vertical wind profiles.

The ID method is well covered in the COMET module *Anticipating Strom Structure and Evolution (COMET, 1996)*. Try some of the examples in the module as exercises to perfect your technique to predict supercell motion.

Exercises in the Comet Module *Anticipating Storm Structure and Evolution*

Objective 12

Describe the physical mechanisms that determine the motion of multicell convection.

a. How does low-level shear and cold pool interactions affect multicell propagation?

b. How does low-level convergence affect multicell propagation?

c. How do boundary interactions affect multicell propagation?

d. How does variations in stability affect multicell propagation?

Multicell Storm Propagation

Multicell storms, comprising the great majority of thunderstorms, are defined as a group of cells in close enough proximity to share a common cold pool and precipitation area. They have been observed in almost all known combinations of shear and buoyancy and include everything from a small collection of ordinary cells to an organized Mesoscale Convective System (MCS) large enough to be influenced by the Coriolis force. Multicell storms may consist solely of simple ordinary cells, or they may also contain embedded supercells. Since multicell storms contain such a wide variety of configurations, multiple mechanisms may exist for determining their movement. However, the linear organization of most multicell storms near the leading edge of their cold pools (also called outflow boundaries) suggests that the cold pool is instrumental in initiating new convection. As a result, the cold pool invokes a propagation vector in a direction which results in a motion that deviates from the mean steering layer flow. These mechanisms include, but are not limited to:

- shear-cold pool interactions
- low-level convergence

- instability gradients
- three-dimensional boundary interactions

Shear-cold Pool Interactions

Since multicell storms have been observed more frequently as shear increases, the role of shear on multicell propagation is important to consider. Rotunno et al. (1988; henceforth referred to as RKW88) developed a theory, based on numerical simulations, to explain the process by which shear interacts with a multicell cold-pool boundary to enhance or suppress lifting. According to RKW88, preferential new cell development occurs on the flank of a multicell storm where the shear vector is directed in a positive sense relative to the orientation of the boundary.

Lifting of Air by Cold Pool

To further explain how shear is considered important, it is necessary to show how a cold pool lifts air at first without the presence of environmental shear. In all situations where a cold pool forms, a density gradient develops along its leading edge. This gradient in density, or buoyancy, induces a horizontal circulation with descending air on the cold side and ascending air on the warm side (Figure 4-12). The ascending air ahead of the gust front lifts up and over the cold dome. It then may become caught in the descending part of the circulation limiting its net vertical lifting. If the LFC was at the height of LFC1 (Fig. 4-12), convective initiation is likely. However, the lifting fails to reach a higher level, LFC2 (Fig. 4-12). Further lifting of the environmental air to LFC2 can only be realized if the cold dome depth increased at some distance away from the leading edge. Therefore, in the absence of shear, and if all other factors are equal,

no portion of a pre-existing cold pool is favored to initiate convection.

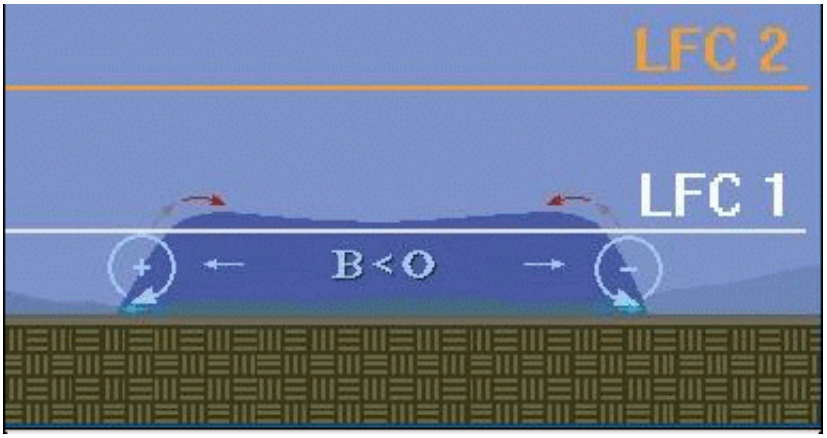

Figure 4-12. Depiction of lifting environmental air relative to two Levels of Free Convection (LFC). Adapted from COMET (1996).

Shear and Cold Pool Lifting

Add shear to the environment and, according to RKW88, the shear interacts with the cold pool to increase (decrease) the lifting on the downshear (upshear) side. Take for example the situation where environmental shear is oriented downshear (or positively) with respect to the outflow boundary (Figure 4-13).

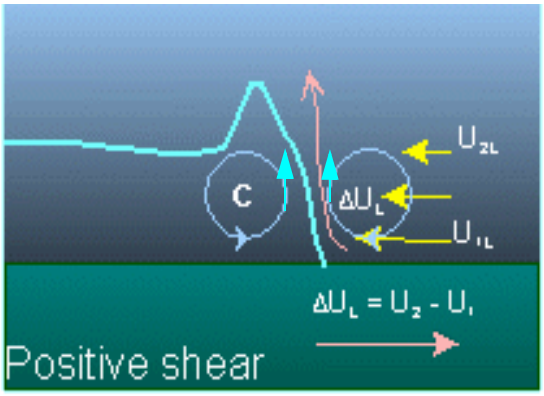

Figure 4-13. Schematic of positive environmental shear interacting with a cold pool boundary (blue perimeter). The yellow arrows indicate boundary-orthogonal wind vectors from U1 (bottom) to U2 (top). The value UL indicates the velocity difference and the orange horizontal arrow is the environmental shear vector. The red vertically pointing arrow represents a hypothetical environmental airparcel trajectory lifting over the boundary.

The positive horizontal vorticity inherent in the environmental shear and the negative horizontal vorticity along the boundary constructively interfere with each other to promote a vertically oriented deep lifting zone. Conversely, on the upshear side of a multicell cold pool (Figure 4-14), the environmental shear is now pointed in a negative direction with respect to the cold pool. In this case, the enviromental horizontal vorticity destructively interferes with that of the cold pool boundary, decreasing the net vertical displacement of the lifted air.

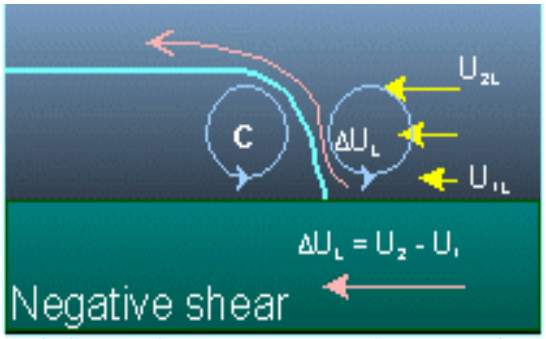

Figure 4-14. Similar to Figure 4-13 except for a negative shear example.

In the framework of RKW88 theory, new cell development is favored on the downshear side of a multicell cold pool. The depth of the shear layer to be calculated when considering this theory is on the order of the depth of the boundary, approximately two kilometers.

Uncertainties in Shear-cold Pool Lifting

There are some uncertainties when using the RKW88 theory for multicell propagation. One involves the proper depth of the shear and whether it should be a function of the LFC height, boundary height, or another benchmark. RKW88 encourages using a shear layer around 3 km deep. However, their suggestion is based on idealized simulations. As will be discussed later, new theories argue for increasing the shear layer depth

beyond that of RKW88 when attempting to describe squall line longevity (Coniglio and Stensrud, 2001). Also, we do not know how dominant this mechanism is in modulating multicell propagation, versus other mechanisms such as instability gradients, interactions with strong low-level winds and boundary interactions. We will be discussing these considerations next.

Gradients in Instability

Gradients in instability can modulate the propagation of multicells, even without the shear/cold pool balance. Richardson (1999) successfully modeled the effect an instability gradient has on the propagation of a multicell line. Not surprisingly, new cell development was favored on the side of the cold pool with a lower LFC. Eventually, the favored side produced a larger cold pool and continued propagation into the instability gradient as shown in Figure 4-15. To summarize, Richardson (1999) showed the importance of forcing the multicell propagation vector toward higher regions of instability as measured by higher CAPE and lower LFC.

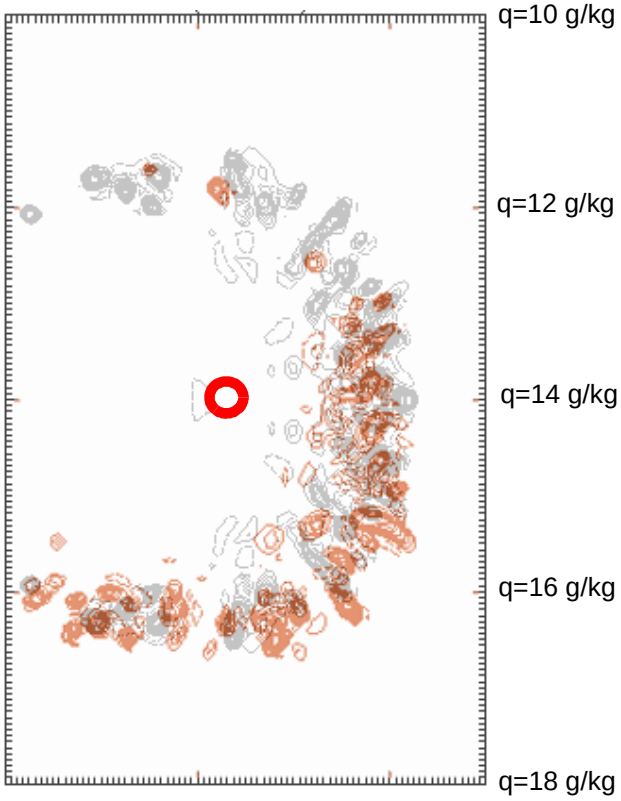

Figure 4-15. Contours of vertical velocity at Z=4.6 km AGL from a model simulation of multicell convection three hours after initiation. The gray contours are from a homogeneous mixing ratio run of 14 g/kg while the brown contours are from a model run with a southward directed gradient in mixing ratios whose values are labeled on the right side of this figure. The red circle is the location of storm initiation in a storm-relative frame of reference. Adapted from Richardson (1999).

System-relative Low-level Flow

Other factors that may affect multicell propagation include strong low-level convergence where the low-level jet impinges on the cold pool. Strong ascent of the low-level jet over the cold pool promotes new cell growth and therefore, over time, the multicell complex begins to move with a component of motion toward the low-level jet. In fact, Corfidi et al. (1996) found that most Mesoscale Convective Complexes (MCC) propagation vectors were equal and opposite in magnitude to the presence of a low-level jet centered near 850 mb (Fig. 4-16). When the propagation vector was added to the convective steering-layer flow, the

total motion vector correlated well with the observed MCC motion. Thus, the term 'Corfidi vector' was coined to describe the expected motion vector of an MCC. The correct term is actually called the MBE vector (Corfidi 1998). To estimate the MBE vector, add the mean 850-300 mb wind to the negative of the low-level wind at the level of the strongest wind (usually around 850mb). An example of this is shown in Figure 4-17.

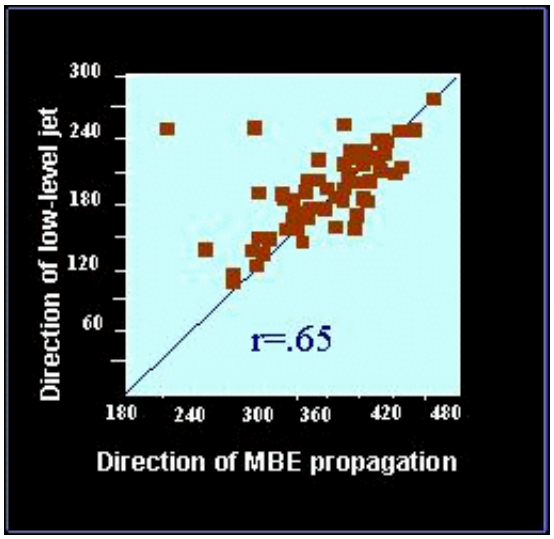

Figure 4-16. Scatterplot of Mesoscale Convective Complex observed direction of propagation and the 850 mb low-level jet direction. Adapted from Corfidi et al. (1996).

Limitations to the MBE Technique

There are several limitations in using the MBE vector technique in MCSs. A significant number of MCSs exhibit a rapid forward propagation component in the presence of low-level inflow that would yield a much different motion vector by the standard MBE technique. For example, a unidirectional vertical wind profile would typically yield very slow MBE vectors yet a significant number of MCSs exhibit rapid motions under this kind of wind profile. Another limitation, or issue, is picking the proper depth in which to calculate a convective steering current. The mean wind should be representative of observed ordinary cell motions. If the

analyzed mean wind disagrees, then the MBE vector calculations will be inaccurate. Also, the MBE technique assumes the existence of the low-level jet with maximum winds at the 850 mb level. If the low-level jet is maximized at a different level, the MBE technique may need to be adjusted to account for this variation. Finally, MCSs are large enough such that they may span a mesoscale gradient in wind fields. The MBE technique, applied in different areas of an MCS, may yield different results. One example would be a situation where the low-level jet is directed to only part of the MCS.

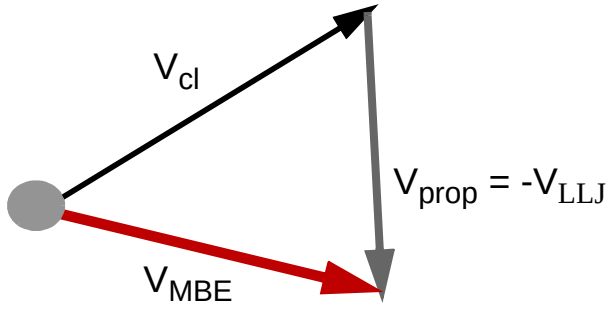

Figure 4-17. A schematic representation of the MBE vectors adapted from Corfidi et al. (1996). V_{cl} represents the mean convective steering-layer flow, V_{prop} is the propagation vector, V_{LLJ} is the low-level jet vector, and V_{MBE} is the motion of the mesoscale convective complex.

Boundary Interactions With Other Boundaries or Topography

Interactions with topography (Petersen et al., 1999) and other boundaries (Purdom, 1976; Wilson and Schreiber, 1986; Mahoney, 1988; Fankhauser et al., 1995; Hane et al., 1997; Koch and Ray, 1997) affect the propagation component of multicell storms by focusing new convection at these interaction points. In fact, Mahoney (1988) derived vertical motions up to 16 m/s and updrafts as high as 2 km above ground level during boundary collisions. Convective initiation was found to be very likely after boundary collisions. According to Koch and Ray (1997), convection initiated on more than 50% of all boundary interactions in Colorado and North Carolina for typical summertime

environments in both states (Fig. 4-18). It follows that a multicell convective cold pool interacting with other boundaries may initiate new convection to become part of the original multicell complex and, therefore, lead to a propagation vector in the direction of the boundary interaction. Intersecting

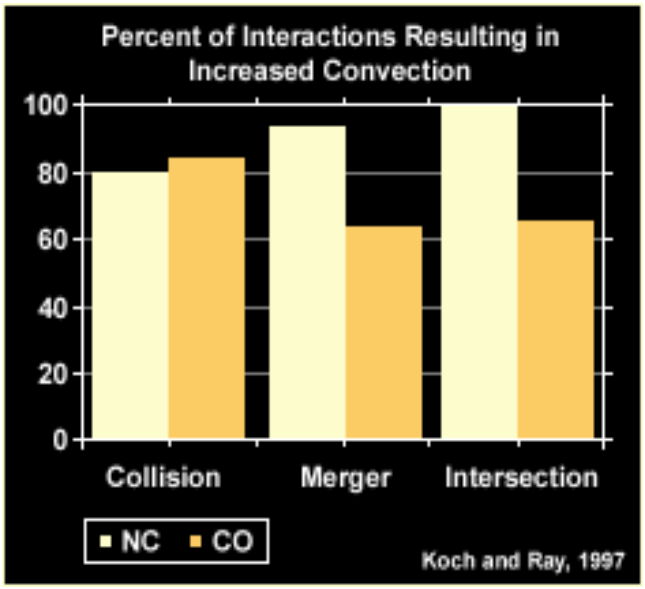

Figure 4-18. Probabilities of convective initiation directly resulting from the interaction of surface boundaries for a typical summertime environment based on field studies in Colorado and North Carolina. Adapted from Koch and Ray (1997).

boundaries frequently ‘anchor’ multicell convection resulting in large rainfalls and flash flooding. Weaver (1979) documented multicell motions in the presence of boundary triple points. Multicell storm motions tended to match the motions of the triple point rather than the convective steering-layer flow (Fig. 4-19).

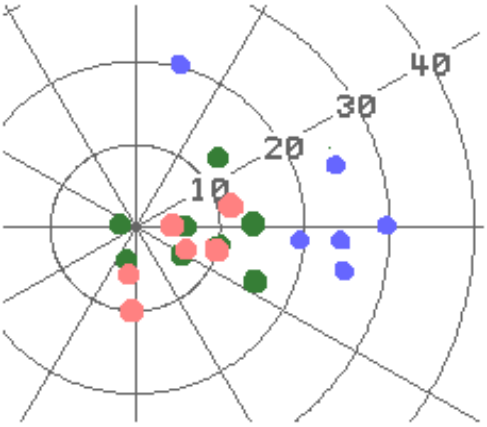

Figure 4-19. A plot of steering-layer flow (blue dots), boundary triple point motions (green dots) and multicell motions (red dots) for several events documented by Weaver (1979).

More Than One Propagation Mechanism at Once

Any combination of these mechanisms may affect multicell propagation, even on the same multicell storm. For example, shear/cold pool interactions may result in a downshear propagation component on one side of a multicell storm while boundary interactions may result in another propagation component. The effect can be a splitting of the multicell complex with a downshear and upshear propagation component.

Objective 13

For multicell convection, describe how interactions with the near-storm environment affects its longevity.

- **a. What is the role of instability?**
- **b. What is the role of low-level shear?**
- **c. What is the role of deep-layered shear?**
- **d. Identify factors which determine the length of time for squall lines to evolve from downshear- to upshear-tilted structures.**
- **e. What component of shear should be considered when assessing the role shear contributes to MCS longevity?**

The Role of Convective Instability

The influence of convective instability (in terms of CAPE) on the strength of a single thunderstorm has been discussed previously (Objectives 3-4). For larger convective systems (like squall lines and bow echoes), the buoyancy of the environment plays a similarly important role. Without sufficient environmental buoyancy, air parcels can not reach their LFC, a crucial part of the thunderstorm development process. As thunderstorm cells begin to organize into multicell lines, a steady source of unstable and positively buoyant air in the inflow portion of the line is necessary (in addition to the other factors) for the convective system to sustain itself.

Johns and Hirt (1987) studied warm-season derechos (large squall lines with embedded bow echoes that produce a long swath of damaging winds). They found that derecho environments were characterized by copious moisture at low levels and extreme convective instability (avg. LI of -9), although lesser instability accompanied the "strong" 500 mb shortwave troughs in their data set. Similarly, Johns et al. (1990) examined 14 very intense derechos during the months of June and July and found that CAPE values were generally greater than 2400 J/kg near the genesis region, but increased to an average CAPE maximum of 4500 J/kg as the convective system moved eastward.

Weisman (1993) studied the effects of CAPE and shear on numerically simulated squall lines and bow echoes and established a minimum threshold of CAPE of 2000 J/kg for long-lived systems.

Evans and Doswell (2001) also studied CAPE distributions in squall lines (via proximity soundings)

and found a much greater range of values for CAPE for derecho events. They found that in most of the cases that were weakly-forced (WF), the instability (and CAPE) were generally larger than in those cases where the forcing was "strong" (SF) (Fig. 4-20 on page 54). For strongly forced events (SF), there were a number of derecho systems that developed and persisted in CAPE environments with low values of CAPE. A few derechos even developed and persisted within regions of conditionally stable surface air.

Thus, squall lines have been observed over a wide range of environmental CAPE (and vertical wind shear). For any given CAPE, the intensity and longevity of linear convective systems seem to increase with increasing synoptic scale forcing, which includes depth and strength of the vertical wind shear.

Vertical Wind Shear Effects and Relationship With CAPE in Squall Line Systems.

Bluestein and Jain (1985) studied squall lines in Oklahoma and found that the magnitude of the vertical wind shear on average was slightly stronger for severe lines than for the non-severe lines. In their study, the average CAPE for severe lines was significantly larger than for the non-severe lines (2260 J/kg versus 1372 J/kg), which agrees with other studies (Fig. 4-21).

Numerical cloud modeling simulations of long-lived severe squall lines in *An MCS Matrix* (COMET, 1999) explored the storm-scale evolution in the development and maintenance of long-lived multicellular systems (such as bow echoes). The effects of environmental shear (in the lowest 2.5 to 5 km AGL) in balance with the surface cold-pool circulation were determined to have the most influence to squall line/bow echo longevity. Vertical

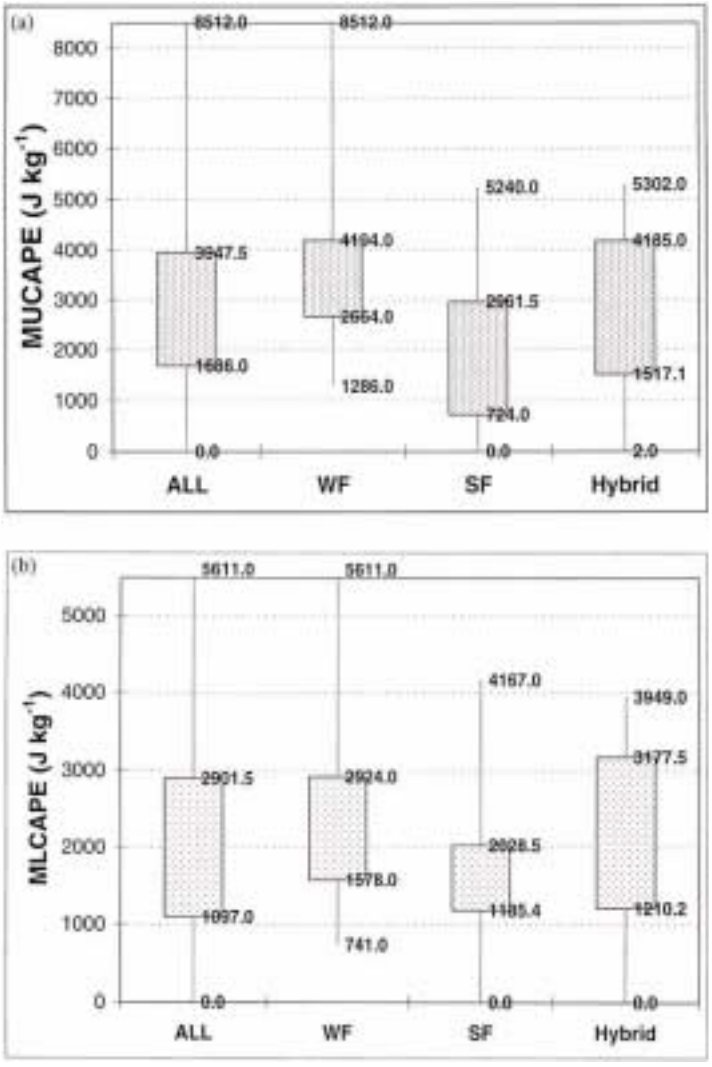

Figure 4-20. A box and whiskers plot of a) Most Unstable CAPE, and b) Mixed Layer CAPE versus the type of derecho observed by Evans and Doswell (2001). The label SF on the x-axis indicates parameters count for only strong synoptic forcing, WF indicates weak synoptic forcing, Hybrid indicates those derechos with aspects of both strong and weak synoptic forcing. The label ALL represents parameters for all derechos.

wind shear values of 20 ms^{-1} or greater were determined to be the “optimum" value for domain-averaged precipitation. Weisman (1993) indicated that significant, long-lived bow echoes evolved when the cold-pool circulation became stronger than the low-level shear in the simulations, allowing the system to develop an upshear-tilted structure (Fig. 4-22) . This structure, which developed after several hours in the simulations, showed a

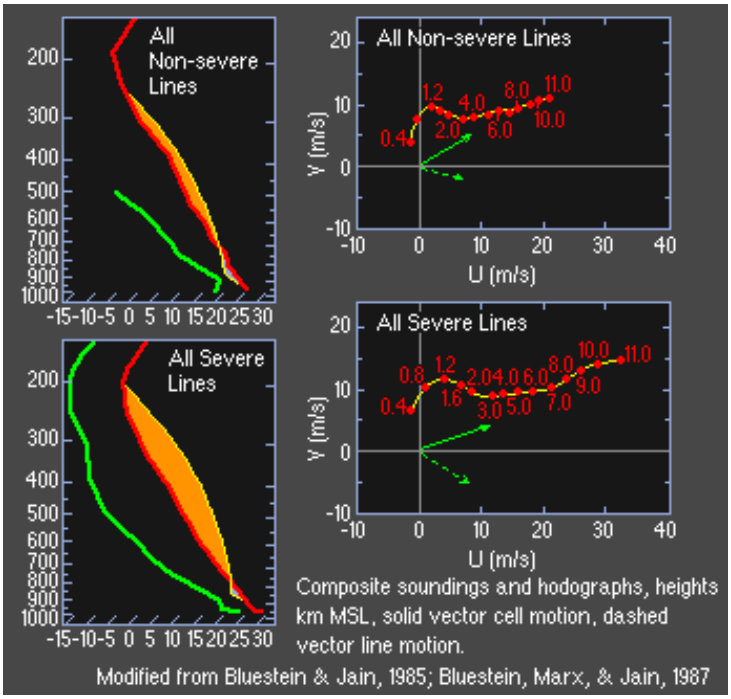

Figure 4-21. Comparison of mean vertical thermodynamic and wind profiles for severe and non-severe squall lines.

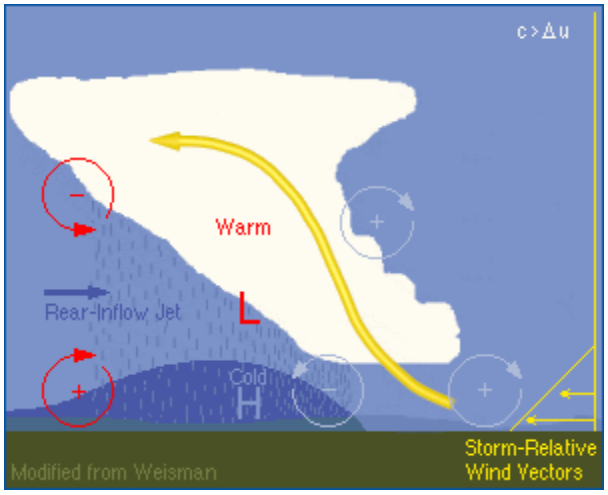

Figure 4-22. Convection developing along a leading edge of a cold pool with an upshear tilted structure (COMET, 1999).

sloped, warm, front-to-rear ascending current developing above the cold pool due to large environmental CAPE. This situation causes the development of a strong rear-inflow jet (RIJ), which, if it remains elevated and approaches the leading edge of the system, can contribute to increasing (upright) low-level updrafts as well as deepening the surface cold pool, thereby strengthening the

overall system even further (Fig. 4-23). Objective 14 explains the RIJ in more detail.

Shear, CAPE and the Development of Bow Echoes

From the modeling simulations, it was suggested that strong low-level vertical wind shear (roughly in the 0-2 km layer) and correspondingly high values of CAPE were needed to support the development of 3-D mesoscale features such as elevated RIJs and bookend vortices within the convective system. These features tended to establish forced lifting along the leading edge of the system and keep strong convective cells located there.

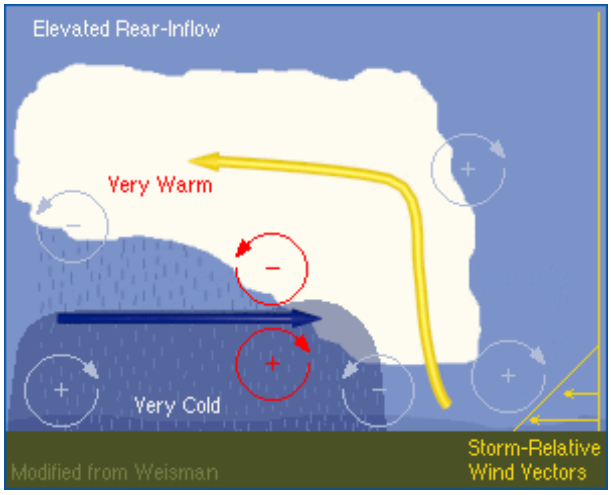

Figure 4-23. Development of an elevated rear-inflow jet in squall line simulations (COMET, 1999).

Latest on Cold Pool Strength and Shear

Evans and Doswell (2001) did not find a clear relationship between cold pool strength and low-level shear. Their data showed that DCAPE (used as a proxy for cold pool strength) and shear were not positively correlated (Figure 4-24). However, they were unable to test with their observations the assertion that the elevated RIJ was necessary to re-balance the cold pool/shear circulation (Weisman, 1993).

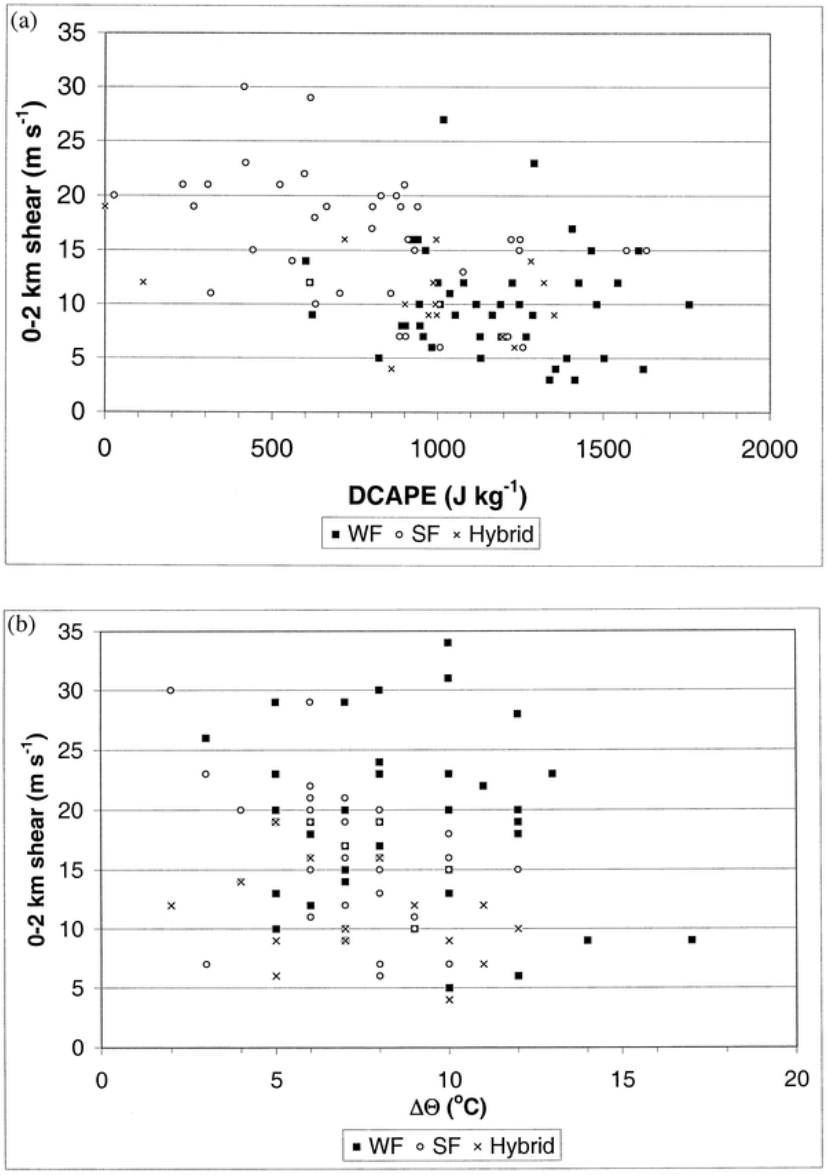

Figure 4-24. Scatterplot of a) DCAPE vs 0-2 km shear vector magnitude and b) surface $\Delta\theta$ across the cold pool vs 0-2 km shear. Adapted from Evans and Doswell (2001).

Role of Deep-layer Shear

Another shear-related factor likely contributing to squall line strength is deep layer shear and low-level system-relative flow. Evans and Doswell (2001) results showed that the mean winds in the 0-6 km layer and the 0-2 km system-relative inflow were stronger because system speeds were faster for derecho events in Mesoscale Convective Systems (MCSs) as compared to MCSs that did not produce derechos (Figure 4-25 and Figure 4-26).

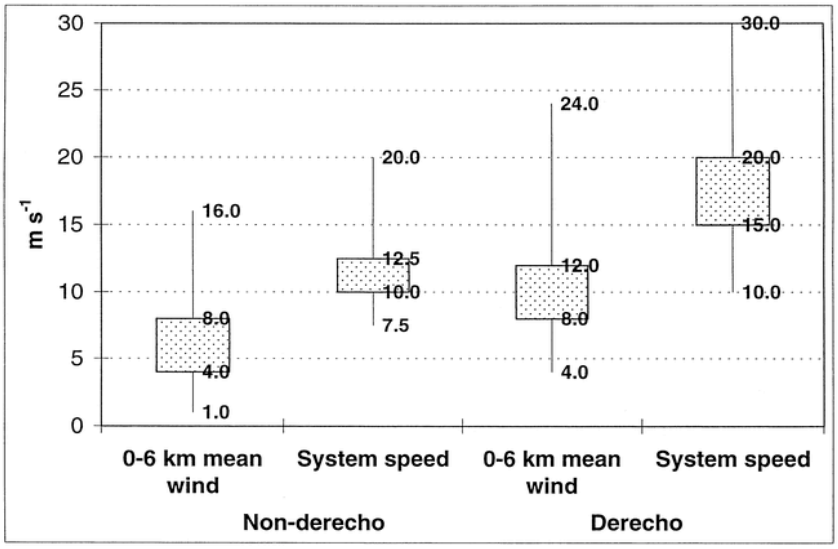

Figure 4-25. Box and whiskers plot of mean wind and system speed for severe and non-severe derechos. The shaded areas represent the 25th and 75th % quartiles while the end-points are the maxima and minima. Taken from Evans and Doswell (2001).

The 0-2 km system-relative flow was stronger in the strongest derechos likely due to faster forward speed and low-level convergence in the squall lines. The midlevel system-relative winds did not show much difference between derecho and non-derecho events.

In a MM5 simulation of 12 progressive derechos, Coniglio and Stensrud (2001) showed that middle to upper-level shear above the surface cold pool was critical in sustaining squall line structure over longer periods.

Thus, the results of Coniglio and Stensrud (2001) and the operational data sets in Evans and Doswell (2001) suggest that, in similar thermodynamic environments and weak forcing, it is the strength of the mean wind which appears to distinguish between derecho and non-derecho MCS environments. The mean wind and low-level convergence modulates low-level system-relative

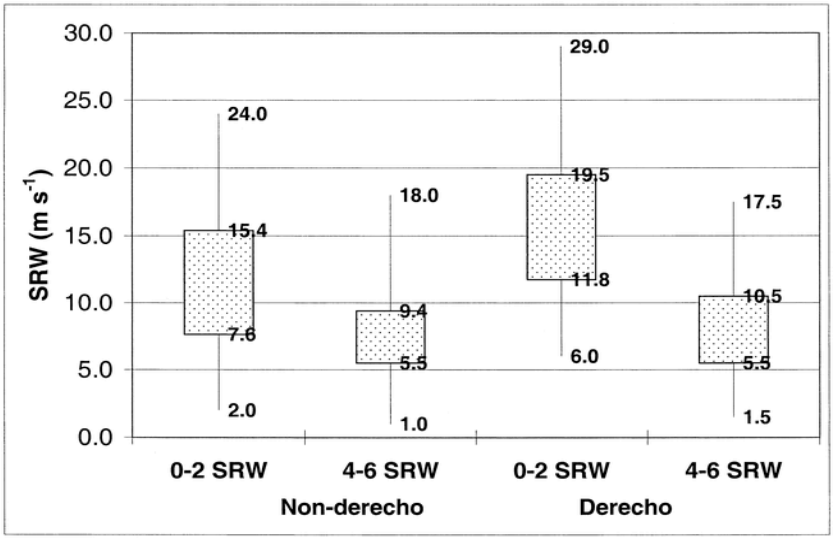

Figure 4-26. Similar to Figure 4-25, except for storm-relative winds.

flow, which also depends on the forward speed of the surface cold pool.

Inverse Relationship Between CAPE and Shear

To summarize, the intensity and longevity of squall lines and bow echoes occur within a wide range of environmental conditions and shear/buoyancy parameters. As in supercell environments, for stronger synoptic forcing, deep layer shear is usually stronger and CAPE is smaller. The converse holds true as well; in weaker synoptic forcing, higher CAPE (and DCAPE) are necessary to maintain the strong winds at the surface. Thus, there is a greater dependence, in weak (0-6 km) flow situations, on strong downdrafts and cold pools for maintaining severe surface winds.

Objective 14

Describe the role of the Rear-Inflow Jet (RIJ) in squall line intensity.

a. What mechanisms form the RIJ?

b. How does shear affect the strength of the RIJ?

c. How does instability affect the strength of the RIJ?

Definition of a Rear-Inflow Jet (RIJ)

The Rear-Inflow Jet (RIJ) is characterized by strong post-gust front winds that originate in the trailing stratiform rainfall region of a squall line at the top of the cold pool and that blow toward the leading edge. The RIJ can either descend or remain elevated during its transit to the leading edge. It represents the mature stage of an MCS and may also signify the beginning of its demise. However, a significant number of squall lines continue to show significant longevity and severity after the RIJ forms.

A Brief Backround

Observational studies such as Smull and Houze (1987) found that the RIJ was generated locally by a convective complex when significant flow accelerations were observed from rear to front in the majority of observed squall lines. Smull and Houze (1987) further suggested that the RIJ may be forced by a hydrostatically generated low under the trailing anvil region just behind the leading edge. They observed numerous examples of long-lived squall lines with persistent RIJs. Fovell and Ogura (1988) noted that the strongest squall lines in their simulations tended to have the strongest cold pools, which would have lead to the most imbalance between the cold pool and environmental circulations. Apparently, the theory proposed by Rotunno et al. (1988) needed modification to account for this contradiction. Further 3-D numerical simulations suggested to Weisman (1992) that an elevated RIJ toward the leading edge can restore cold pool circulation balance with the environmental shear, maintaining the longevity of a squall line. Elevated RIJs, according to Weisman (1992), arise when the circulation of the overturning anvil is well matched to that of the rear of the cold pool. Starting around 4 km AGL, the jet horizontally extends to the front of the squall line and just above the cold pool. Since the bottom edge of

the RIJ resides above the cold pool, the circulations tend to destructively interfere with each other. This process diminishes the strength of the cold pool in terms of circulation and therefore reduces the dominance of the cold pool over the environmental shear. Owing to the difficult nature of observing this interaction, there have been no statistical studies that can either support or refute this theory. Weisman (1992) theorized that high values of shear and buoyancy caused elevated RIJs. However, as was previously noted, Evans and Doswell (2001) observed the parameter space of shear and buoyancy of derechos to be much larger than the similar parameter space for simulated elevated RIJs (Weisman, 1992). What is not known is whether an elevated RIJ is required to produce a derecho.

While some uncertainty exists as to the relationship between an elevated RIJ and a long-lived severe squall line, we present further details of the Weisman (1992) theory to explain the dynamics and forecasting implications of the RIJ. It is highly recommended to review the COMET module on *Mesoscale Convective Systems: Squall Lines and Bow Echoes* (COMET, 1999) for further details on RIJs.

The Dynamics of an RIJ

To explain the dynamics of the RIJ, we will start with a mature squall line schematic (Figure 4-27). As a squall line matures, high-level anvil material begins to stream from the leading edge back into the rear side of the squall line (represented by the yellow trajectory in Fig. 4-27). Loaded with small- and medium-sized hydrometeors that have not previously fallen out in the leading edge, the anvil begins to drop its precipitation which results in the trailing stratiform precipitation. The anvil material is also warming the upper-troposphere through the

injection of huge amounts of latent heat released in the updraft along the leading edge. This heat acts to hydrostatically lower the pressure beneath the anvil but above the cold pool (marked by a 'L' in Figure 4-27). A hydrostatic high still exists near ground-level in the cold pool, dominating any lowering of pressure caused by anvil material aloft. Speaking in terms of pressure dynamics, the anvil-induced low induces air to laterally flow in from both the front and rear sides of the squall line. Although the updraft tends to limit the amount of air coming in from the front, there is no obstruction from the rear side and air begins to flow, initiating the RIJ. Presumably, the strongest midlevel low resides underneath the thickest part of the anvil just behind the deep updraft along the leading edge of the squall line. Therefore, the RIJ accelerates until it is just behind the updraft. We next discuss the strength of the acceleration and the factors that govern the slope of the RIJ.

Buoyancy Effects on the RIJ

The strength of the low underneath the anvil depends on the intensity of the net warming in the anvil. Looking at Figure 4-28, the squall line

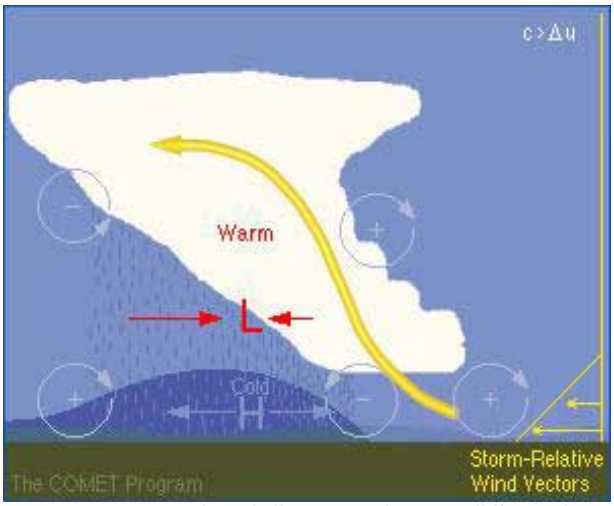

Figure 4-27. A cross-sectional diagram of a squall line taken from the COMET MCS module (1998). The relevant labels include the updraft trajecory (yellow arrow), the midlevel low (red L), the inflow into the low (red arrows) and the cold pool high (blue H).

updraft with the greatest positive temperature excess is the one utilizing the greatest CAPE. Note the hypothetical sounding profile and the temperature excess of the updraft parcel from the environment. The result of higher CAPE is typically a stronger RIJ. Typically with environments of large CAPE, lapse rates and differences from the surface to midlevels tend to be larger, promoting stronger cold pools. From a vorticity argument, a stronger cold pool circulation to the rear of the squall line works with a more buoyant anvil aloft to generate strong midlevel horizontal inflow that forces the RIJ from the rear of the squall line.

Shear Effects on the RIJ

Given the same buoyancy for updrafts and cold pools, shear can modulate the intensity of the RIJ. According to numerical simulations, as shear increases, the updraft along the leading edge becomes more erect and stronger. More heat is pumped into the anvil just behind the leading edge causing a stronger hydrostatic low in the midlevels. The more intense precipitation from the stronger updraft is hypothesized to create a stronger cold pool as well.

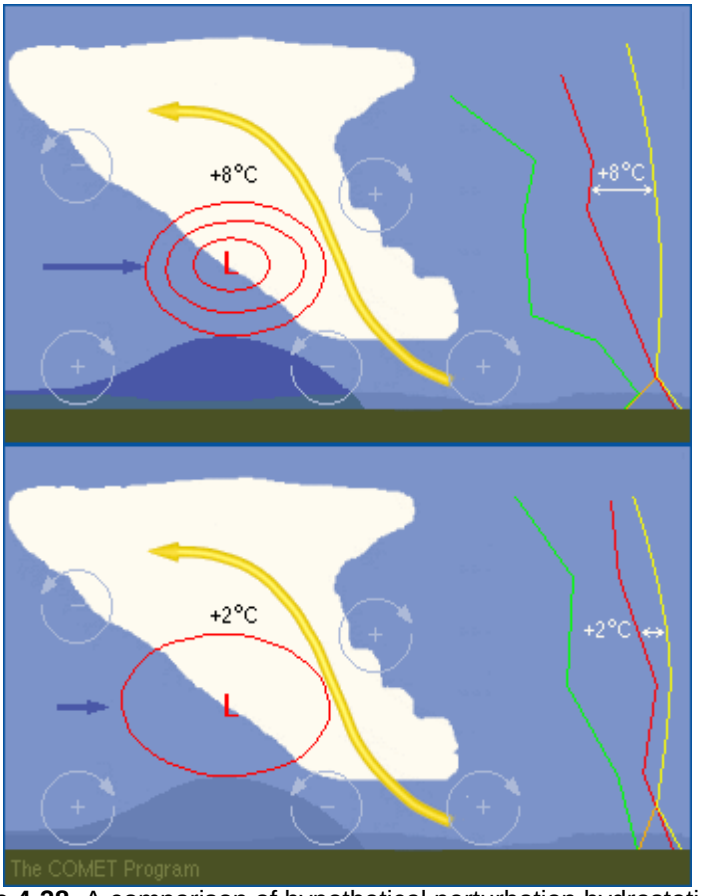

Figure 4-28. A comparison of hypothetical perturbation hydrostatic isobars (red contours) is presented for a high CAPE (top panel) and a low CAPE case (bottom panel). The blue arrow left of the isobars is intended to illustrate the relative magnitude of the rear inflow jet. From the COMET MCS module (COMET, 1999).

Descending vs. Nondescending RIJs

According to simulations proposed by Weisman (1992), the longevity of the squall line may depend on the rear-to-front slope of the RIJ. Although there may be multiple slopes to the RIJs, there are two extremes:

1. A descending RIJ and

2. A nondescending RIJ.

A Descending RIJ

A descending RIJ occurs when the vorticity generated just underneath of the ascending front-to-rear updraft is weaker than the vorticity generated of the opposite sign on the rear edge of the cold dome. In Figure 4-29, the imbalance between the

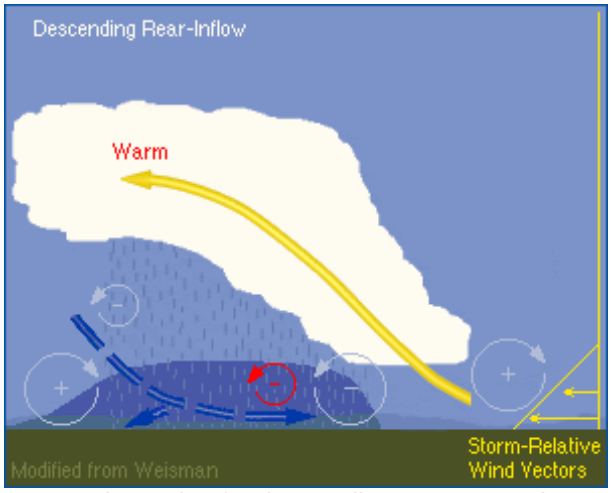

Figure 4-29. A schematic of a descending RIJ. From the COMET MCS module (COMET, 1999).

two circulations can be seen to help force the RIJ downward towards the ground prior to it reaching the leading edge of the gust front. The RIJ then reinforces the vorticity along the leading edge increasing the imbalance between the cold pool and environmental vorticity. The squall line is theorized to become increasingly sloped rearward while weakening. According to simulations by Weisman (1992), this situation occurs with weakening shear (less than 15 m/s over the lowest several km) or if the environmental CAPE falls to less than 1000 J/kg.

Nondescending RIJ

As CAPE and/or shear increases, the vorticity underneath the rearward expanding anvil becomes much larger due to the increased buoyancy within the anvil. The counterrotating vorticity along the back edge of the cold dome does not increase as much. This situation results in the increased buoyancy-induced vorticity under the anvil matching with the cold dome vorticity to invoke a more horizontally oriented RIJ (Fig. 4-30). This nondescending RIJ progresses towards the leading edge of the cold pool with a horizontal vorticity structure that interferes with the spreading cold pool vorticity near the gust front. Thus the

strength of the gust front vorticity drops off to become more balanced with the environment and the squall line updraft retains an upright nature. Squall lines with a nondescending RIJ tended to live longer than their descending RIJ counterparts (Weisman 1992).

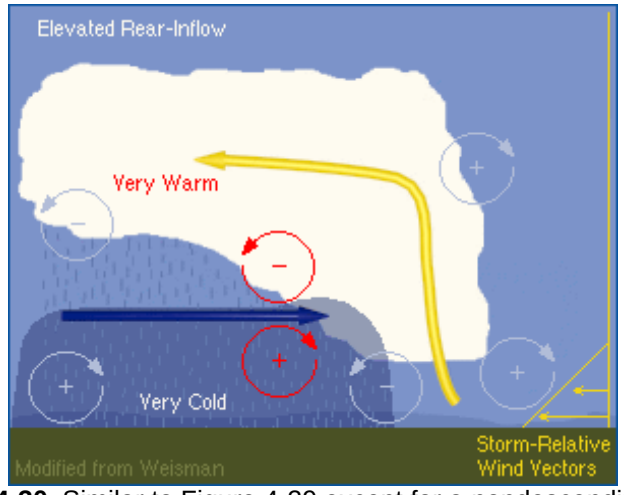

Figure 4-30. Similar to Figure 4-29 except for a nondescending RIJ example. Adapted from Weisman (1992).

Other Mechanisms Leading to Long-lived Damaging Squall Lines

The role of a nondescending RIJ in squall line longevity put forth by Weisman (1992) may not adequately explain the longevity of some severe squall lines in environments exhibiting low values of 0-3 km shear. Other numerical experiments (Xue, 2000; Shapiro, 1992; and Coniglio and Stensrud, 2001) provide evidence that adding shear in a layer above the lowest few km in such a way to yield low gust front-relative storm motion may allow squall lines to persist longer than predicted by shear/cold pool balance theory. In addition, strong synoptic-scale midlevel winds may boost the initiation time and strength of the RIJ. An example would be a cold-season, pre-frontal squall line in a warm sector of a surface cyclone (Johns, 1993).

Impact of Synoptic-scale Midlevel Flow

As mentioned earlier, Evans and Doswell (2001) observed numerous cases of derechos without

high values of either shear or buoyancy. They did notice a relationship between longevity, mean steering-layer winds and low-level storm-relative inflow. The latter relationship is likely due to the fact that derechos move quickly. In addition, strong RIJs may be the result of dynamics beyond that of balancing anvil-level buoyancy with cold pool strength. For example, small amounts of CAPE are sufficient to vertically mix strong, synoptic-scale midlevel winds down to the surface yielding a strong RIJ-like structure.

Therefore it is important not only to look for high values of low-level shear, but also the existence of strong deep-layered shear and strong convective steering-layer flow. As is often the case, the parameter space in which long-lived multicell squall lines are observed is often much larger than simulations suggest.

Objective 15

Identify the characteristics of bow echoes and the mechanisms involved in their formation.

a. **What are the characteristics of squall lines with line-end vortices (bow echoes)?**
b. **What are the characteristics of severe bow echoes?**
c. **What is the mechanism that creates line end vortices in a bow echo?**
d. **What is the role of the Coriolis force in organizing bow echoes?**

Line-end Vortices

In the mature phase of a well-organized squall line system, it is not uncommon to observe three-dimensional features such as elevated RIJs, line-end vortices, and even supercells. Line-end vortices (often called bookend vortices) typically, by

definition, evolve at the end of the line or at breaks within the line. The development of these features can alter the subsequent evolution fo the system.

In the numerical simulations presented in the *MCS module* (COMET, 1999), line-end vortices typically developed between 2-4 h into the lifetime of the convective system, just behind the zone of most active convection. The vortex at the northern end of the system had cyclonic rotation, while the vortex at the southern end of the system rotated anticyclonically (for a north-south oriented squall line propagating toward the east in the Northern Hemisphere; see Figure 4-31).

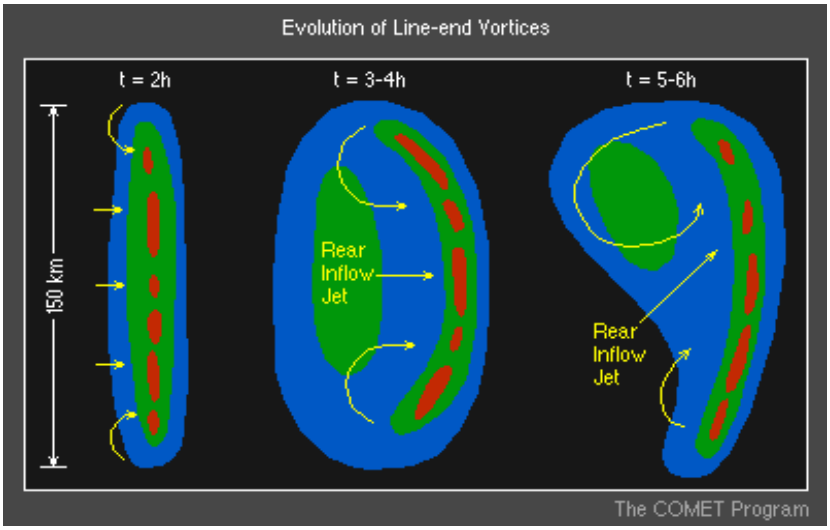

Figure 4-31. Development of a cyclonic "bookend" vortex in a squall line simulation. From the COMET *MCS module* (COMET, 1999).

Cyclonic vs. Anticyclonic Line-end Vortex

The cyclonic vortex at the northern end of line tends to become stronger and larger than the southern, anticyclonic vortex (according to the simulations). As this occurs, the convective system becomes asymmetric, with most of the stratiform precipitation region found behind the northern end of the system and the strongest leading-line convective cells found near the southern end. In weak-to-moderate shear environments, the domi-

nant northern line-end vortex was typically observed to move rearward with time. When the ambient shear was strongest and the system updraft remained erect longest, the line end vortices tended to remain closer to the leading line convection.

In the simulations, the impact of midlevel convergence in the presence of Coriolis forcing acted to strengthen the northern cyclonic bookend vortex, but weaken the anticyclonic bookend vortex with time. The strengthening of the cyclonic bookend vortex is thought to produce the symmetric-to-asymmetric evolution that characterizes most long-lived MCSs.

Mesoscale Convective Vortex (MCV)

The dominant cyclonic vortex can last well beyond the lifetime of the originating convective system and is often referred to as a Mesoscale Convective Vortex (MCV). In some cases, MCVs have been documented to last for several days, helping to trigger subsequent convective outbreaks.

Line-end Vortices are Downdrafts

Since the line-end vortices typically develop within the downdraft portion of the squall line, they are not usually associated with supercell tornadoes. However, because they can enhance the strength of the RIJ between the vortices, line-end vortices are a source of increased downdraft and stronger surface winds. In this way, they can contribute to the spin-up of tornadoes at the leading edge of the system outflow.

Distance Between Line-end Vortices

According to the *MCS module* (COMET, 1999), the smaller the distance between the line-end vortices, the more enhancement to the midlevel flow between vortices, which strengthens the RIJ. The descent of this enhanced RIJ to the surface is

hypothesized to produce the extreme surface winds associated with bow echoes. (Figure 4-32).

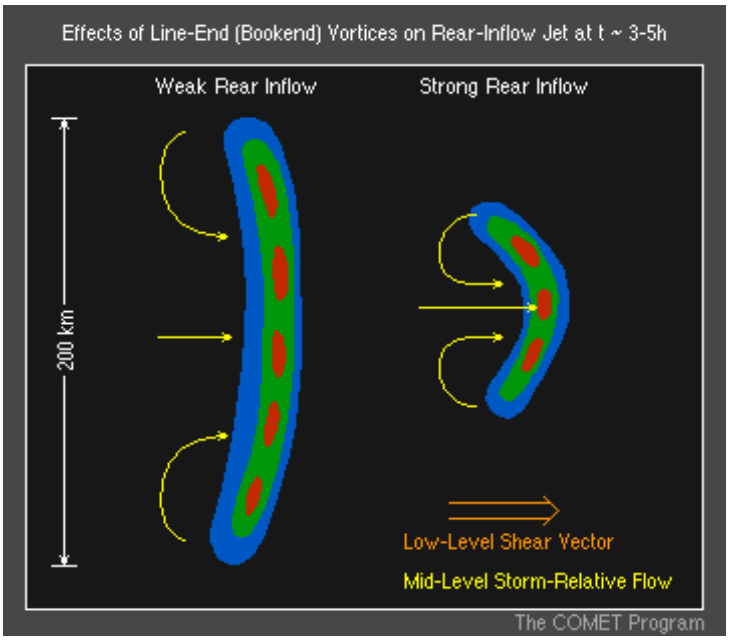

Figure 4-32. Effect of bookend vortices on the strength of an RIJ. From COMET (1999).

Characteristics of Severe Bow Echoes

Fujita (1978) coined the term “bow echo” to describe the radar presentation of long (20-120 km) bow-shaped systems of convective cells noted for producing long swaths of strong surface winds. Bow echoes are typically observed on radar as an accelerating portion of a squall line and are usually concave-shaped.

Bow echoes often occur from either isolated storms or within much larger convective systems (such as squall lines). When multiple bow echoes are observed within a squall line, the radar signature is referred to as a Line Echo Wave Pattern (LEWP).

LEWPs

Many features of bow echo evolution which cause the typical LEWP structure (such as the rotating comma head and the cyclonic/anticyclonic rotating vortices) are based on the conceptual model from

Fujita (1978; Figure 4-33). Fujita found that the initial echo started as a strong isolated cell or a small line of cells. The initial cells then evolved into a symmetric bow-shaped segment of cells over a period of a couple of hours, and eventually into a comma-shaped echo over several hours.

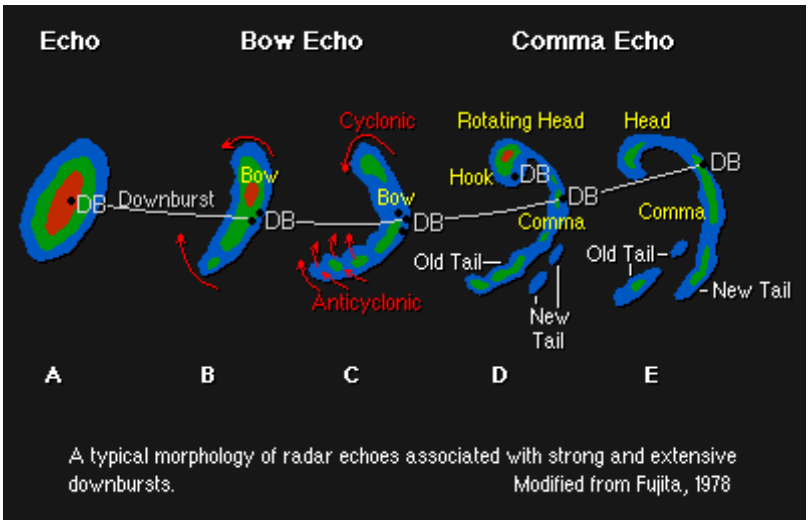

Figure 4-33. Conceptual model of a bow echo evolution. Adapted from Fujita (1978) and COMET (1999).

Rear-inflow Notch on Radar

Another radar characteristic of bow echoes noted in the simulations and observed in WSR-88D imagery is the development of the weak echo notch, sometimes referred to as a Rear-Inflow Notch (RIN). The RIN is located well behind the core of the bow (Figure 4-34), and it often signifies the location of a strong RIJ. The RINs were frequently observed along the trailing edge of each individual bowing segment, signifying a region of evaporatively-cooled lower Θ_e air being channeled toward the leading edge of the bow (Przybylinski and Schmocker 1993). In large, distinctive bow echoes, multiple RINs, or weak echo channels, can be observed on radar imagery (Przybylinski, 1995). These RINs may be locations where the RIJ is descending to the ground. When the RIJ descends to the ground near the leading edge of the bow, it can create a swath of damaging surface

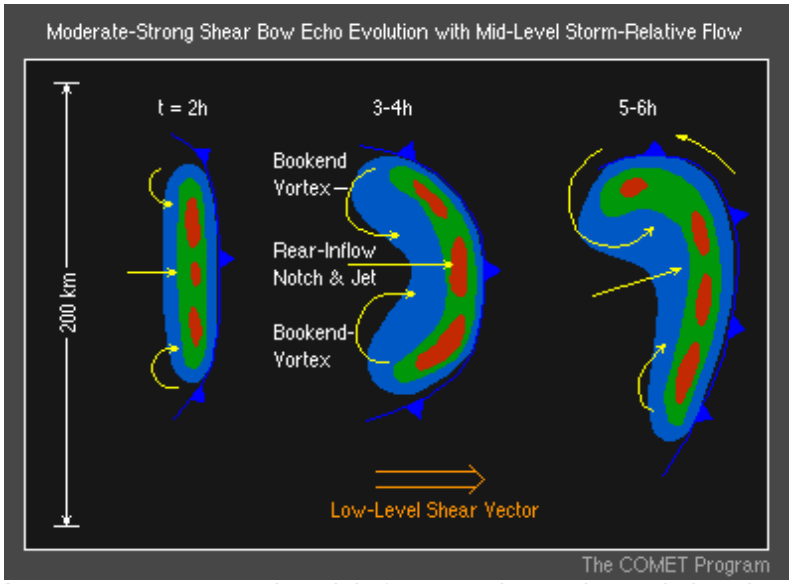

Figure 4-34. Conceptual model of a strong bow echo evolution showing bookend vortices and development of a Rear-Inflow Notch (RIN). From COMET (1999).

winds. Weak tornadoes are often observed just north of this surface jet core.

Cross-section of Bow Echoes

Vertical cross-sections in the core of mature bow echo simulations (Figure 4-35) revealed a strong, vertically erect updraft at the leading edge of the system; a strong, elevated RIJ impinging just behind the updraft region before descending rapidly to the surface; and a system-scale updraft that turned rapidly rearward aloft, feeding into the stratiform precipitation region.

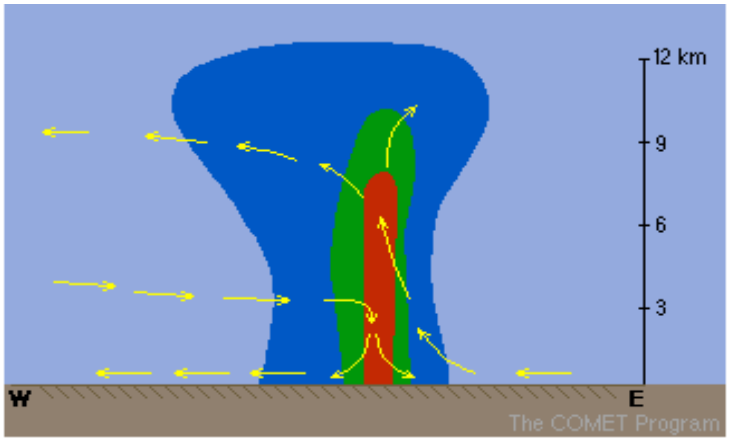

Figure 4-35. Schematic of a vertical cross-section through a mature bow echo. From COMET (1999).

Midaltitude Radial Convergence

Observations of a midaltitude radial convergence signature (MARC) on radar has been noted by Przybylinski (1998) as a precursor to the descent of the elevated RIJ. Enhanced velocity differentials (areas of strong convergence) are often located just downwind of high reflectivity cores along the leading edge of the convective line (Figure 4-36). Persistent areas of MARC greater than 25 m/s at 3-5 km (AGL) can sometimes provide lead time for the first report of wind damage (often before a well-defined bow echo w/bookend vortex develops).

Supercell Transition to Bow Echo

Supercells are also observed occasionally within the larger bow echo structure. In some cases, an isolated supercell is observed to evolve directly into a bow echo as the supercell decays. This type of evolution is typically seen with HP supercells (Fig. 4-37 on page 75).

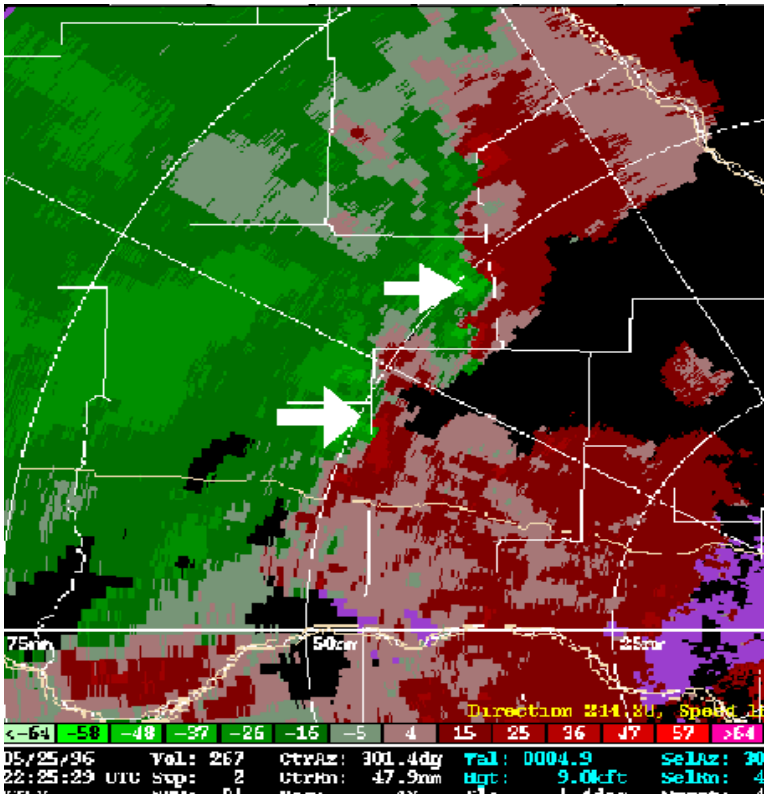

Figure 4-36. An example of a midaltitude radial convergence zone in a bow echo as seen in the Storm-Relative Velocity Map product.

Radar Morphologies of Bow Echoes

Przybylinski and DeCaire (1986) identified four types of radar reflectivity signatures associated with derechos (23 cases examined). These signatures are depicted nicely on Page 8 of the Bow Echoes section under *Conceptual Models on the MCS web site* (COMET, 1999). All of these types of signatures indicate intense, low-level reflectivity gradients along the leading edge of the bow with pronounced RINs and/or weak echo channels on the trailing end of the bow.

Other Bow Echo Signatures

Other bow echo radar signatures include the MARC signature (discussed in previous section). More examples will be given in the accompanying teletraining session.

Bow Echo Propagation

Numerical simulations (Weisman, 1993) found that bow echoes tended to propagate in the direction of the mean low-level vertical wind shear vector at a speed influenced by the cold pool propagation. Since the cold pools in bow echoes were often exceptionally strong, their propagation speed was often much faster than nearby convective cells or systems.

Bow Echo Environments

As was discussed in Lesson 2, severe bow echoes (such as derechos) are observed to occur over a wide range of CAPE and shear environments. Bow echo patterns have been studied by many researchers including Johns and Hirt (1987), Johns (1993), and Przybylinski (1995). During the warm season, development of so-called "progressive derechos" (Johns, 1993) are common across portions of the central and eastern United States. These derechos were defined as short bow echo segments that move parallel to a quasi-stationary front in the general direction of the mean flow (Figure 4-38). Progressive derecho environments consist of a strong warm air advection pattern

somewhere near the initiation region of the system, a thermodynamic environment characterized by relatively strong midlevel winds, a large amount of low-level moisture, a steep low- to midlevel lapse rate, and correspondingly high CAPE. Some sort of east-west oriented boundary is also usually present.

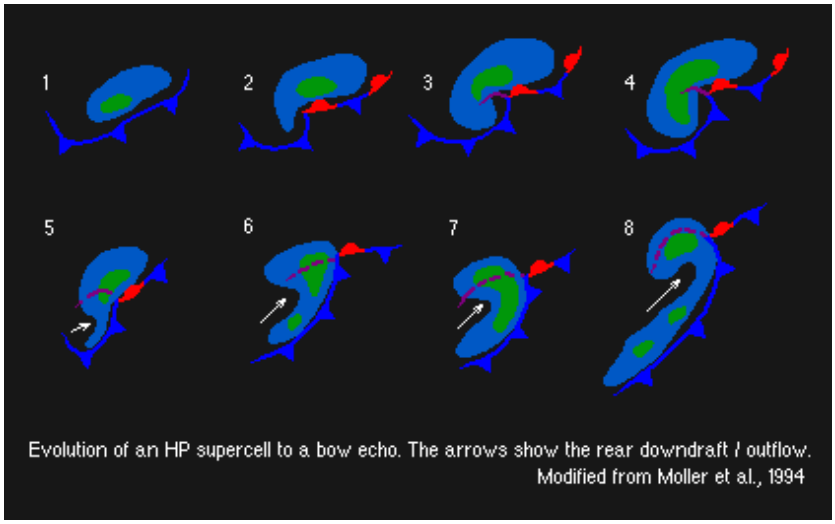

Figure 4-37. Depiction of an evolution of an HP supercell to a bow echo (COMET, 1999).

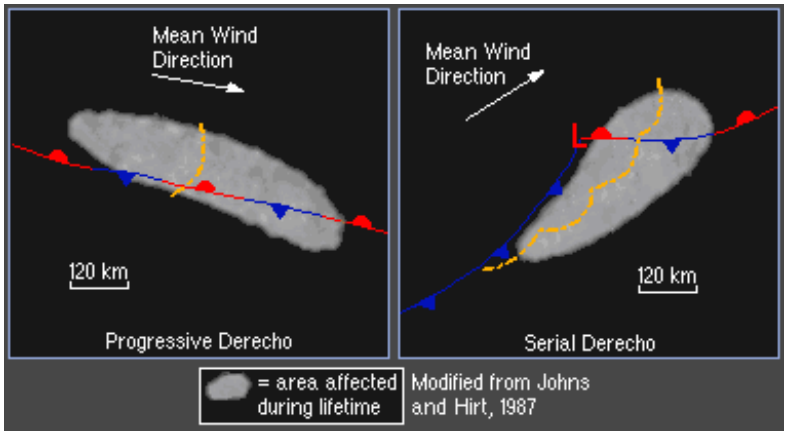

Figure 4-38. Two types of Derecho patterns (COMET, 1999).

Progressive Derechos

Due to the orientation of the leading edge of the surface cold pool (or gust front) normal to the mean wind direction, system-relative flow is maximized in the downshear direction of progressive derechos. The cold pools (once generated by the

stratiform region) for these types of bow echoes will thus discretely propagate and move rapidly in the direction of the mean wind as a result of momentum transfer and because boundary layer convergence is maximized on the downshear side of the cold pool. The entire convective system associated with progressive derechos typically moves faster than the mean wind (Johns and Hirt, 1987).

Serial Derechos

The serial derecho (Fig. 4-38) consists of an extensive squall line where the angle oriented between the mean wind and squall line axis is relatively small (Johns and Hirt, 1987). The squall line typically moves normal to the mean wind at speeds of 30 kts or less, while the individual LEWPs and bow echoes move rapidly in the direction of the mean wind and tend to be most frequent near the northern end of the line. Serial derechos may contain supercells because the patterns which produce these types of derechos, the so-called "dynamic pattern" (Johns, 1993), is typically associated with a strong, migrating low pressure system and has many characteristics of the classic Great Plains tornado outbreak pattern. One slight difference in the dynamic bow-echo synoptic pattern, which actually occurs more frequently in the fall/winter season, is that the low-level jet is usually more parallel to the middle and upper-level jets (Duke and Rogash, 1992). Because both supercells and severe bow echoes require strong vertical wind shear, both storm types often occur in close proximity to one another, or evolve from one structure to the other, during their lifetime.

Mechanisms Leading To Line-end Vortex Formation

The mechanisms that create the line-end vortices (also bookend vortices) can be explained by the similar vortex tilting processes that form mesocyclones and mesoanticyclones in supercell storms.

For supercell storms in westerly vertical wind shear, cyclonic (anticyclonic) vertical vorticity is generated when the vortex lines are tilted by an updraft on the cell's south (north) side. For a bow echo, however, the cyclonic vertical vorticity lies on the north side (Fig. 4-32), completely reverse to that of isolated supercells.

Downward Tilting in Westerly Shear

A downdraft tilting horizontal vorticity embedded in westerly environmental shear is one possible explanation of this phenomenon. In Figure 4-39, cyclonic vorticity would be generated on the left (north) side of the downdraft which fits well with the bow echo conceptual model.

Upward Tilting in Easterly Shear

Easterly shear is another possible configuration where an updraft may tilt vortex lines to create a cyclonic vortex on the north side (Fig. 4-40). Where does easterly shear come from in an environment of westerly shear? The leading side of the cold pool is one very significant place where easterly shear is generated. Air just above the leading edge of the cold pool develops vorticity consistent with easterly shear along the cold pool interface. That same air is being lifted most strongly along the deepest part of the cold pool and therefore, strong vortex tilting on either side develops the couplet of rotation consistent with bookend vortices (Fig. 4-40).

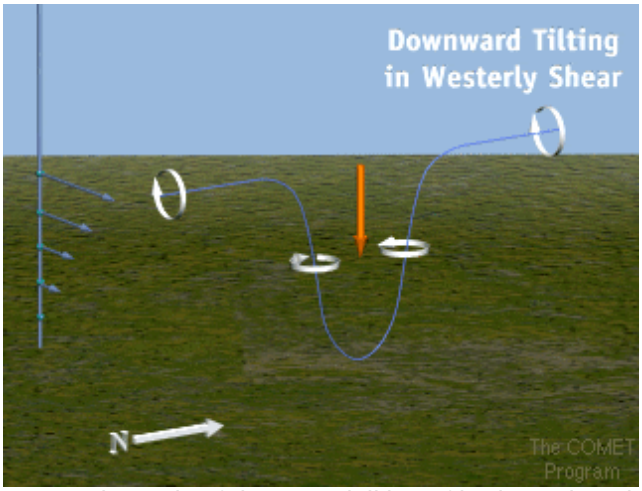

Figure 4-39. Schematic of downward tilting of horizontal vorticity in westerly shear. From COMET (1999).

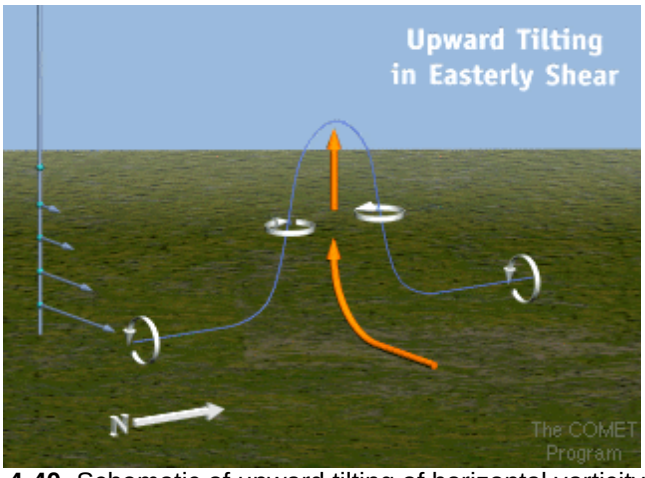

Figure 4-40. Schematic of upward tilting of horizontal vorticity in easterly shear. From COMET (1999).

Both Processes may be at Work in Bow Echoes

Both of these processes conceivably can generate the observed line-end vortices. Downward tilting of the westerly shear in the environment may occur from the rear of the bow echo. Alternatively, lifting of internally generated vorticity along the top interface of the cold pool may also generate these vortices. Through analysis of simulations, Weisman (1993) believes it is the upward tilting of vorticity on either side of the building cold air dome that is largely responsible for the line-end vortices (Fig. 4-41).

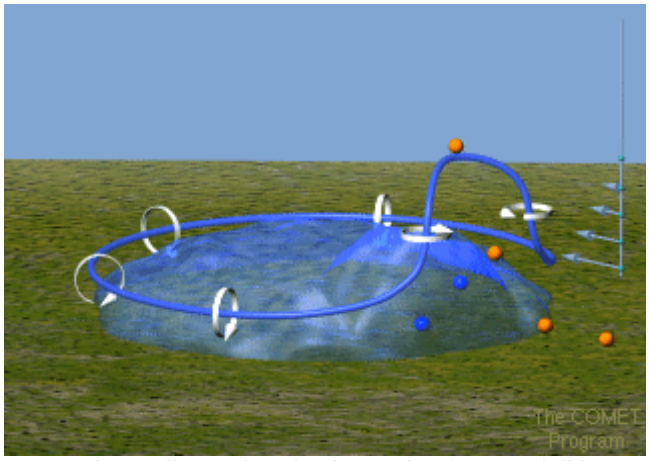

Figure 4-41. Three-dimensional schematic of upward tilting of vortex lines around a localized deep cold pool. From COMET (1999).

The Influence of the Coriolis Force on Bow Echoes.

Over the first half of a bow echo lifespan (<3 hours), the Coriolis force is too weak to influence internal flow fields. If the bow echo flow fields persist for more than a few hours, the integrated effects of the Coriolis force begins to noticeably alter its shape. Pure divergence at anvil-level begins to acquire an anticyclonic component to it. The same process also creates anticyclonic curvature in the flow within the cold pool while cyclonic curvature increases in the midlevel hydrostatic low above the cold pool. Eventually, the northern (southern) line-end vortex strengthens (weakens).

Summary

This lesson can be summarized into four parts which include:

- An understanding of the currently known physical mechanisms behind ordinary-cell, multicell, and supercell motion.
- Factors that affect the longevity of multicells, which include all convection comprising of more than one updraft sharing a common cold pool and precipitation shield.
- The effect of the RIJ on squall line intensity.

- The characteristics of bow echoes.

Motion of Convection

The first part of this lesson has concentrated on explaining our current understanding of the physical mechanisms behind the motion of ordinary cells, supercells and multicell convection. Ordinary cells generally move with a “steering-layer” wind (typically calculated using the mean of the 0-6 km winds). Cyclonically (anticyclonically) rotating supercells move with one component along the mean steering-layer wind and the other (propagation) component to the right (left) of and orthogonal to the 0-6 km shear vector. The magnitude of the propagation component varies anywhere from 3-8 m/s. Multicell storms, consisting of more than one individual ordinary or supercell updraft, also have a propagation vector off the mean wind. Multiple mechanisms may influence the propagation vector predominantly including these factors:

- Shear/cold pool interactions
- Horizontal convective stability variations
- Boundary interactions
- Cold pool/low-level jet interactions

Multicell Longevity

The second part of this lesson discussed environmental and storm-induced factors modulating the lifetime of a multicell cluster such as a squall line. Rotunno et al. (1988) asserted that a balance between the horizontal vorticity along the cold pool boundary and the vorticity inherent in a 0-2 km environmental shear layer is optimal for enhancing strong updrafts needed to maintain a long-lived squall line. Evans and Doswell (2001) did not find the cold pool/shear balance theory to be a factor in observed derecho environments. Derechos are typically associated with long-lived squall lines.

Coniglio and Stensrud (2001) found that deep tropospheric shear was more important than low-level shear in maintaining squall lines. Needless to say, the factors governing the longevity of squall lines are still a controversial subject. There are, however, common environmental parameters including strong convective steering-layer winds, adequate convective instability, and moderate-to-strong deep 0-6 km shear that accompany long-lived severe squall lines (Evans and Doswell, 2001).

RIJs

Rear-Inflow Jets (RIJs) are common with large, linear multcell storms (squall lines). However, numerical simulations suggest the RIJs do not descend in the most severe squall lines (Weisman, 1992). According to Weisman (1992), most squall lines become upshear-tilted as the cold pool dominates environmental shear. A nondescending RIJ restores the balance, allowing the squall line updraft to remain vertically erect for longer periods of time. Nondescending RIJs are found in environments where shear and CAPE are high.

Bow Echoes

Squall line segments exhibiting line-end vortices and a localized RIJ in between the vortices and directed toward the leading edge are often called bow echoes. A series of bow echoes are called Line Echo Wave Patterns (LEWPs). Bow echoes intensify the RIJ between the vortices often leading to localized areas of maximum wind damage. Small tornadoes may occur just to the left of the maximum wind in an RIJ given enough low-level helicity and instability in the environment. The line-end vortices in bow echoes develop by either tilting negative storm-induced vorticity at the top end of the cold pool from the storm updraft, and/or by tilting positive environmental vorticity downward by the downdraft in the back end of a bow echo.

Appendix A: References

Blanchard, D.O., 1998: Assessing the vertical distribution of convective available potential energy. *Wea. and Forecasting*, **13**, 870-877.

Bluestein, H.B., and M.H. Jain, 1985: Formation of mesoscale lines of precipitation: Severe squall lines in Oklahoma during the spring. *J. Atmos. Sci*., **42**, 1711-1732.

Browning, K. A., and F. H. Ludlum, 1962: Airflow in convective storms. *Quart. J. Roy. Meteor. Soc.*, **88**, 117-135.

Bunkers, M. J., B. A. Klimowski, J. W. Zeitler, R. L. Thompson, and M. L. Weisman, 2000: Predicting supercell motion using a new hodograph technique. *Wea. Forecasting*, **15**, 61-79.

Byers, H. R., and R. Braham, 1949: The Thunderstorm. Govt. Printing Office, Washington, DC, 287 pp.

COMET, 1999: Mesoscale Convective Systems: Squall Lines and Bow Echoes. Online training module, http://www.meted.ucar.edu/convectn/mcs/index.htm.

____, 1996: Anticipating convective storm structure and evolution. CD-ROM.

____, 1995: A convective storm matrix: Buoyancy/shear dependencies. CD-ROM.

Coniglio, M. C., and D. J. Stensrud, 2001: Simulation of a Progressive derecho using composite initial conditions. *Monthly Weather Review*, **129**, 1593—1616.

Corfidi, S.F., J.H. Merritt, and J.M. Fritsch, 1996: Predicting the movement of mesoscale convective complexes. *Wea. Forecasting*, **11**, 41-46.

Crook, N.A., 1996: Sensitivity of moist convection forced by boundary layer processes to low-level thermodynamic fields. Mon. Wea. Rev., 124, 1767-1785.

Davies, J.M., 1993: Hourly helicity, instability and EHI in forecasting supercell tornadoes. Preprints, 17th Conf. on Severe Local Storms, St. Louis, Amer. Meteor. Soc., 107-111.

——, and R. H. Johns, 1993: Some wind and instability parameters associated with strong and violent tornadoes. *Part I: Wind shear and helicity. The Tornado: Its Structure, Dynamics, Prediction, and Hazards, Geophys. Monogr.*, No. 79, Amer. Geophys. Union, 573–582.

Davies-Jones, R., 1984: Streamwise vorticity: The origin of updraft rotation in supercell storms. *J. Atmos. Sci.*, **41**, 2991-3006.

___, Burgess and M. Foster, 1990: Test of helicity as a tornado forecast parameter. Preprints, *16th Conf on Severe Local Storms*, Kananaskis Park, Alberta, Amer. Meteor. Soc., 588-592.

Duke, J. W., and J.A. Rogash, 1992: Multiscale review of the development and early evolution of the 9 April 1991 derecho. *Wea. Forecasting*, **7**, 623—635.

Edwards, R., and R. L. Thompson, 2000: RUC2 Supercell proximity soundings, part II: An independent assessment of supercell forecast parameters. Preprints, *20th Conf. on Severe Local Storms*, Orlando, Amer. Meteor. Soc., 435-438.

Emanuel, K. A., 1994: Atmospheric Convection. Oxford University Press, 883 pp.

Evans, J. S. and C. A. Doswell III, 2001: Examination of Derecho environments using proximity soundings. *Wea. Forecasting*, **16**, 329-342.

Fankhauser, J.C., N.A. Crook, J. Tuttle, L.J. Miller, C.G. Wade, 1995: Initiation of deep convection along boundary layer convergence lines in a semitropical environment. *Monthly Weather Review*:, **123**, 291–314.

Fawbush, E. J., and R. C. Miller, 1954: The types of airmasses in which North American tornadoes form. *Bull. Amer. Soc.*, **35**, 154-165.

Foster, D. S., 1958: Thunderstorm gusts compared with computed downdraft speeds. *Mon. Wea. Rev.*, **86**, 91-94.

Fovell, Robert G., Yoshi Ogura, 1988: Numerical simulation of a midlatitude squall line in two dimensions. *J. Atmos. Sci.*, **45**, 3846–3879.

Fujita, T.T., 1978: Manual of downburst identification for project NIMROD. SMRP Research Paper No. 156, 104 pp.

Gilmore, M. S. , and L. J. Wicker, 1998: The influence of midtropospheric dryness on supercell morphology and evolution, *Mon. Wea. Rev.*, **126**, 943-958.

Grant, B. N., 1995: Elevated Cold-Sector Severe Thunderstorms: A Preliminary Study. *National Weather Digest* , **19:4**, 25-31.

Hane, Carl E., Howard B. Bluestein, Todd M. Crawford, Michael E. Baldwin, Robert M. Rabin, 1997: Severe thunderstorm development in relation to alongdryline variability: A case study. *Mon. Wea. Rev.*, **125**, 231–251.

Hart, J. A., and W. Korotky, 1991: The SHARP workstation v1.50 users guide. National Weather Service, NOAA, 30pp.

Johns R. H., and C.A. Doswell III, 1992: Severe Local Storms Forecasting. *Symposium of Weather Forecasting*, 72nd AMS Annual Meeting, Atlanta.

Johns, R.H. and W.D. Hirt, 1987: Derechos: widespread convectively induced windstorms. *Wea. Forecasting*, **2**, 32-49.

Johns, R.H., 1993: Meteorological conditions associated with bow echo development in convective storms. *Wea. Forecasting*, **8**, 294-300.

Johns, R.H., J.M. Davies, and P.W. Leftwich, 1990: An examination of the relationship of 0-2 km agl "positive" wind shear to potential buoyant energy in strong and violent tornado situations. *16th Conf on Severe Local Storms*, Kananaskis Park, Alberta, 593-598.

Kerr, B.W., and G.L. Darkow, 1996: Storm-relative winds and helicity in tornadic thunderstorm environments. *Wea. Forecasting*, **11**, 489-505.

____, C. A. Ray, 1997: Mesoanalysis of summertime convergence zones in central and eastern North Carolina. *Wea. Forecasting*, **12**, 56–77

Maddox, R. A., 1976: An evaluation of tornado proximity wind and stability data. *Mon. Wea. Rev.*, **104**, 133–142.

Mahoney, W.P. III, 1988: Gust front characteristics and the kinematics associated with interacting thunderstorm outflows. *Mon. Wea. Rev.*, **116**, 1474-1491.

McCaul, E. W., and M. L. Weisman, 1996: The dependence of simulated storm structure on variations in the shapes of environment buoyancy and shear profiles. Preprints, *18th Conf. on Severe Local Storms*, San Francisco, CA, Amer. Meteor. Soc., 718-722.

Petersen, W.r A., L. D. Carey, S. A. Rutledge, J. C. Knievel, R. H. Johnson, N. J. Doesken, T. B. McKee, T. Vonder Haar, and J. F. Weaver, 1999: Mesoscale and Radar Observations of the Fort Collins Flash Flood of 28 July 1997. *Bull. Amer. Meteor. Soc*., **80**, 191–216.

Przybylinski, R.W., 1995: The bow echo: observations, numerical simulations, and severe weather detection methods. *Wea. Forecasting*, **10**, 203-218.

____, 1995: The bow echo: Observations, numerical simulations, and severe weather detection methods. *Wea. Forecasting*, **10**, 203-218.

____, and G.K. Schmocker, 1993: The evolution of a widespread convective wind storm event over central and eastern Missouri. Preprints, *13th Conf. on Weather Analysis and Forecasting*, Vienna, VA, Amer. Meteor. Soc., 461-465.

____, T.J. Shea, D.L. Ferry, E.H. Goetsch, R.R. Czys, and N.E. Wescott, 1993: Doppler radar observations of high-precipitation supercells over the mid-Mississippi Valley region. Preprints, *17th Conf. on Severe Local Storms*, St. Louis, MO, Amer. Meteor. Soc., 158-163.

____., and D. M. DeCaire, 1985: Radar signatures associated with the derecho. One type of mesoscale convective system. Preprints *14th Conf. on Severe Local Storms*, Indianapolis, IN, Amer. Meteor. Soc., 228-231.

Purdom, J. F. W., 1976: Some uses of high resolution GOES imagery in the mesoscale forecasting of convection and its behavior. *Mon. Wea. Rev.*, 104, 1474–1483

RTM-230, 2000: Skew T Log P Diagram and Sounding Analysis, National Weather Service Training Center Remote Training Module.

Rasmussen, E. N., 2001: Refined supercell and tornado forecast parameters from the 1992 baseline climatology. Unpublished web-based paper.

____, and D. Blanchard, 1998: A baseline climatology of sounding-derived supercell and tornado forecast parameters. *Wea and Forecasting*, **13**, 1148-1164.

____, S. Richardson, J. Straka, P. Markowski, and D. Blanchard, 1998: The association of significant tornadoes with a baroclinic boundary on 2 June 1995. *Mon. Wea. Rev.*, **128**, 174-191.

____, and R. B. Wilhelmson 1983: Relationships between storm characteristics and 1200 GMT hodographs, low-level shear, and stability. preprints, *13th conf. on Severe Local Storms,* Tulsa, OK, Amer. Meteor. Soc., J5-J8.

Richardson, Y.P., 1999: The Influence of horizontal variations in vertical shear and low-level moisture on numerically simulated convective storms. Ph.D. Dissertation, School of Meteorology, University of Oklahoma - Norman, 236 pp.

Shapiro, A. 1992. A hydrodynamical model of shear flow over semi-infinite barriers with application to density currents. *J. Atmos. Sci*. **49**, 2293–2305

Smull, Bradley F., R. A. Houze, Jr., 1987: Rear Inflow in Squall Lines with Trailing Stratiform Precipitation. Mon. Wea. Rev., 115, 2869–2889.

Stensrud, D.J., J.V. Cortinas, Jr., and H.E. Brooks, 1997: Discriminating between tornadic and nontornadic thunderstorms using mesoscale model output. *Wea. Forecasting*, **12**, 613-632.

Thompson, R.L., 1996: Supercell tornado forecasts derived from Eta model storm-relative winds. Preprints, *18th Conf. on Severe Local Storms*, San Francisco, CA, AMS, 362-366.

____, 1998: Eta model storm-relative winds associated with tornadic and nontornadic supercells. *Wea. Forecasting*, **13**, 125-137.

Weaver, J. F., 1979: Storm Motion as Related to Boundary-Layer Convergence. *Mon. Wea. Rev.*, **107**, 612–619.

Weisman, M. L., 1993: The Genesis of Severe, Long-Lived Bow Echoes. *J. Atmos. Sci*., **50**, 645–645.

____, 1992: The Role of Convectively Generated Rear-Inflow Jets in the Evolution of Long-Lived Mesoconvective Systems. *J. Atmos. Sci.*, **49**, 1826–1847.

_____., and J. B. Klemp, 1984: The structure and classification of numerically simulated convective storms in directionally varying wind shears. *Mon. Wea. Rev*., **112**, 2479-2498.

_____, and J. B. Klemp, 1982: The dependence of numerically simulated convective storms on vertical wind shear and buoyancy. *Mon. Wea. Rev.*, **110**, 504-520.

Wicker, L. J., and L. Cantrell, 1996: The role of vertical buoyancy distributions in miniature supercells. Preprints, *18th Conf. on Severe Local Storms*, San Francisco, CA, Amer. Met. Soc, 225-229.

Wilson, J.W., 1986: Tornadogenesis by nonprecipitation induced wind shear lines. *Mon. Wea. Rev.*, **114**, 270-284.

____, R. E. Carbone, J. D. Tuttle, and T. D. Keenan, 2001: Tropical island Convection in the Absence of Significant topography. Part II: Nowcasting Storm Evolution. *Mon. Wea. Rev*., **129**, 1507–1525.

____, and D. L. Megenhardt, 1997: Thunderstorm Initiation, Organization, and Lifetime Associated with Florida Boundary Layer Convergence Lines. *Mon. Wea. Rev*. **125**, 1507–1525

____, and W. E. Schreiber, 1986: Initiation of convective storms by radar-observed boundary layer convergent lines. *Mon. Wea. Rev.*, **114**, 2516—2536

Xue, M. 2000. Density currents in two-layer shear flows. *Quart. J. Roy. Atmos. Sci.*, **126**, 1301—1320.

Appendix B: Bibliography

Atkins, N. L. , M. L. Weisman, and L.J. Wicker, 1998: The Influence of Pre-existing Boundaries on Supercell Evolution. *Mon. Wea. Rev.* , **127**, 2910 - 2927.

Bartels, D.L., and R.A. Maddox, 1991: Midlevel cyclonic vortices generated by mesoscale convective systems. *Mon. Wea. Rev.*, **119**, 104-118

Bartha, I., 1994: Development of a decision procedure for forecasting maximum wind gusts associated with thunderstorms. *Met. Appl.,* **1**, 103.

Blanchard, D.O., 1998: Assessing the vertical distribution of convective available potential energy. *Wea. and Forecasting*, **13**, 870-877.

Bluestein, H.B., and M.H. Jain, 1985: Formation of mesoscale lines of precipitation: Severe squall lines in Oklahoma during the spring. *J. Atmos. Sci*., **42**, 1711-1732.

____, and C.R. Parks, 1983: A synoptic and photographic climatology of low-precipitation severe thunderstorms in the southern plains. *Mon. Wea. Rev.*, **111**, 2034-2046.

____, and G.R. Woodall, 1990: Doppler radar analysis of a low-precipitation severe storm. *Mon. Wea. Rev.*, **118**, 1640-1664.

Brandes, E.A., 1990: Evolution and structure of the 6-7 May 1985 mesoscale convective system and associated vortex. *Mon. Wea. Rev.*, **118**, 109-127.

Braun, S.A., and J. P. Monteverdi, 1991: An analysis of a mesocyclone-induced tornado occurrence in northern California. *Wea. Forecasting*, **6**, 13-31.

Brooks, H.E. and R.B. Wilhelmson, 1993: Hodograph curvature and updraft intensity in numerically modeled supercells. *J. Atmos. Sci.*, **50**, 1824-1833.

Brooks, H.E., C.A. Doswell III, M.T. Carr, and J.E. Ruthford, 1996: Preliminary analysis of soundings from VORTEX-95. *Preprints, 18th Conf. On Severe Local Storms*, San Francisco, CA, Amer. Meteor. Soc., 133-136.

Brooks, H.E., C.A. Doswell III and R. Davies-Jones, 1993: Environmental helicity and the maintenance and evolution of low-level mesocyclones. *The Tornado: Its Structure, Dynamics, Prediction and Hazards*, Geophysical Monographs, No. 79, American Geophysical Union, 97-104.

Brooks, H.E., C.A. Doswell III and J. Cooper, 1994: On the Environments of Tornadic and Non-tornadic Mesocyclones. *Wea. Forecasting*, **9**, 606.

Brown, R.A., 1990: Characteristics of supercell hodographs. *Preprints, 16th Conf. on Severe Local Storms*, Kananaskis Park, Alta., Canada, Amer. Meteor. Soc., 30-33.

Brown, R.A., and V.T. Wood, 1991: On the interpretation of single-Doppler velocity patterns within severe thunderstorms. *Wea. Forecasting*, **6**, 32-48.

Browning, K. A., and F. H. Ludlum, 1962: Airflow in convective storms. *Quart. J. Roy. Meteor. Soc.*, **88**, 117-135.

Bunkers, M. J., B. A. Klimowski, J. W. Zeitler, R. L. Thompson, and M. L. Weisman, 2000: Predicting supercell motion using a new hodograph technique. *Wea. Forecasting*, **15**, 61-79.

Burgess, D.W., and L.R. Lemon, 1990: Severe thunderstorm detection by radar. *Radar in Meteorology*, D. Atlas, Ed., Amer. Meteor. Soc., 619-647.

Burgess, D.W., and B.F. Smull, 1990: Doppler radar observations of a bow echo associated with a long-track severe windstorm. *Preprints, 16th Conf. Sev. Loc. Storms*, Amer. Meteor. Soc., 203-208.

Byers, H. R., and R. Braham, 1949: The Thunderstorm. Govt. Printing Office, Washington, DC, 287 pp.

Chisholm, A.J., and J.H. Renick, 1972: The kinematics of multicell and supercell Alberta hailstorms. *Alberta Hail Studies, Research Council of Alberta Hail Studies*, Rep. 72-2, Edmonton, Canada, 24-31.

Colquhoun, J.R., and P.A. Riley, 1996: Relationships between tornado intensity and various wind and thermodynamic variables. *Weather and Forecasting*, **11**, 360-371.

COMET, 1999: Mesoscale Convective Systems: Squall Lines and Bow Echoes. Online training module, http://www.meted.ucar.edu/convectn/mcs/index.htm.

____, 1996: Anticipating convective storm structure and evolution. CD-ROM.

____, 1995: A convective storm matrix: Buoyancy/shear dependencies. CD-ROM.

Coniglio, M. C., and D. J. Stensrud, 2001: Simulation of a Progressive derecho using composite initial conditions. *Monthly Weather Review*, **129**, 1593—1616.

Corfidi, S.F., J.H. Merritt, and J.M. Fritsch, 1996: Predicting the movement of mesoscale convective complexes. *Wea. Forecasting*, **11**, 41-46.

Crook, N.A., 1996: Sensitivity of moist convection forced by boundary layer processes to low-level thermodynamic fields. Mon. Wea. Rev., 124, 1767-1785.

Davies, J.M., 1993: Hourly helicity, instability and EHI in forecasting supercell tornadoes. Preprints, 17th Conf. on Severe Local Storms, St. Louis, Amer. Meteor. Soc., 107-111.

——, and R. H. Johns, 1993: Some wind and instability parameters associated with strong and violent tornadoes. *Part I: Wind shear and helicity. The Tornado: Its Structure, Dynamics, Prediction, and Hazards, Geophys. Monogr.*, No. 79, Amer. Geophys. Union, 573–582.

Davies-Jones, R., 1984: Streamwise vorticity: The origin of updraft rotation in supercell storms. *J. Atmos. Sci.*, **41**, 2991-3006.

___, Burgess and M. Foster, 1990: Test of helicity as a tornado forecast parameter. Preprints, *16th Conf on Severe Local Storms*, Kananaskis Park, Alberta, Amer. Meteor. Soc., 588-592.

Doswell, C. A., III, 1987: The distinction between large-scale and mesoscale contribution to severe convection: A case study example. *Wea. Forecasting*, **2**, 3-16. A training unit on MCCs as they pertain to the severe weather threat, other than heavy precipitation

____, A.R. Moller, and R. Przybylinski, 1990: A unified set of conceptual models for variations on the supercell theme. Preprints, *16th Conf. on Severe Local Storms*, Kananaskis Park, Alta., Canada, Amer. Meteor. Soc., 40-45.

____, M.E. Splitt and M. Kay, 1992: On storm motion and operational assessment of supercell storm potential using hodographs. Preprints, 4th AES/CMOS Workshop on Operational Meteorology, Whistler, B.C., Atmos. Env. Serv./Can. Met. and Ocean. Soc., 245-252.

____, S.J. Weiss, and R.H. Johns, 1993: Tornado Forecasting: A Review. In The Tornado: Its Structure, Dynamics, Prediction, and Hazards, C. Church, D. Burgess, C. Doswell, and R. Davies-Jones, Eds.. Geophysical Monograph 79, Amer. Geophysical Union, Washington, DC. 557-572.

____, and H. Brooks, 1993: Supercell Thunderstorms. Wea. Forecasting, 48, 209.

Droegemeier, K.K., S.M. Lazarus, and R. Davies-Jones, 1993: The influence of helicity on numerically simulated convective storms. Mon. Wea. Rev., 121, 2005-2029.

Duke, J. W., and J.A. Rogash, 1992: Multiscale review of the development and early evolution of the 9 April 1991 derecho. *Wea. Forecasting*, **7**, 623—635.

Edwards, R., and R. L. Thompson, 2000: RUC2 Supercell proximity soundings, part II: An independent assessment of supercell forecast parameters. Preprints, *20th Conf. on Severe Local Storms*, Orlando, Amer. Meteor. Soc., 435-438.

Emanuel, K. A., 1994: Atmospheric Convection. Oxford University Press, 883 pp.

Evans, J. S. and C. A. Doswell III, 2001: Examination of Derecho environments using proximity soundings. *Wea. Forecasting*, **16**, 329-342.

Evenson, E.C., 1993: Utilization of the Bulk Richardson Number, Helicity and Sounding Modification in the Assessment of the Severe Convective Storms of 3 August 1992. *NOAA Tech. Memo. WR-221*, 21 pp.

Fankhauser, J.C., and C.G. Mohr, 1977: Some correlations between various sounding parameters and hailstorm characteristics in northeast Colorado. Preprints, *10th Conf. on Severe Local Storms*, Omaha, NE, Amer. Meteor. Soc., 218-225.

Fankhauser, J.C., N.A. Crook, J. Tuttle, L.J. Miller, C.G. Wade, 1995: Initiation of deep convection along boundary layer convergence lines in a semitropical environment. *Monthly Weather Review*:, **123**, 291–314.

Fawbush, E. J., and R. C. Miller, 1954: The types of airmasses in which North American tornadoes form. *Bull. Amer. Soc.*, **35**, 154-165.

Foster, D. S., 1958: Thunderstorm gusts compared with computed downdraft speeds. *Mon. Wea. Rev.*, **86**, 91-94.

Foster, M.P., A.R. Moller, L.J. Wicker, and L. Cantrell, 1995: The rapid evolution of a tornadic small supercell; observations and simulation. Preprints, *14th Conf. on Weather Analysis and Forecasting*, Dallas, TX, Amer. Meteor. Soc., 323-328.

Fovell, Robert G., Yoshi Ogura, 1988: Numerical simulation of a midlatitude squall line in two dimensions. *J. Atmos. Sci.*, **45**, 3846–3879.

Funk, T.W., K.E. Darmofal, J.D. Kirkpatrick, V. L. DeWald, R.W. Przybylinski, G.K.

Fujita, T.T., 1978: Manual of downburst identification for project NIMROD. SMRP Research Paper No. 156, 104 pp.

Gilmore, M. S. , and L. J. Wicker, 1998: The influence of midtropospheric dryness on supercell morphology and evolution, *Mon. Wea. Rev.*, **126**, 943-958.

Grant, B. N., 1995: Elevated Cold-Sector Severe Thunderstorms: A Preliminary Study. *National Weather Digest* , **19:4**, 25-31.

Hane, Carl E., Howard B. Bluestein, Todd M. Crawford, Michael E. Baldwin, Robert M. Rabin, 1997: Severe thunderstorm development in relation to along-dryline variability: A case study. *Mon. Wea. Rev.*, **125**, 231–251.

Hart, J. A., and W. Korotky, 1991: The SHARP workstation v1.50 users guide. National Weather Service, NOAA, 30pp.

Hill, C.D., 1993: Forecast Problems in the Western Region of the National Weather Service: An Overview. *Wea. Forecasting*, **8**, 158.

Johns R. H., and C.A. Doswell III, 1992: Severe Local Storms Forecasting. *Symposium of Weather Forecasting*, 72nd AMS Annual Meeting, Atlanta.

Johns, R.H., and J.A. Hart, 1993: Differentiating between different types of severe thunderstorm outbreak: A preliminary investigation. Preprints, *17th Conf. On Severe Local Storms*, St. Louis, MO, Amer. Meteor. Soc., 46-50.

Johns, R.H. and W.D. Hirt, 1987: Derechos: widespread convectively induced windstorms. *Wea. Forecasting*, **2**, 32-49.

Johns, R.H., 1993: Meteorological conditions associated with bow echo development in convective storms. *Wea. Forecasting*, **8**, 294-300.

Johns, R.H., J.M. Davies, and P.W. Leftwich, 1990: An examination of the relationship of 0-2 km agl "positive" wind shear to potential buoyant energy in strong and violent tornado situations. *16th Conf on Severe Local Storms*, Kananaskis Park, Alberta, 593-598.

Johnson, R.H., and P.J. Hamilton, 1988: The relationship of surface pressure features to the precipitation and airflow structure of an intense midlatitude squall line. *Mon. Wea. Rev.*, **116**, 1444-1472.

Kennedy, P.C., and S.A. Rutledge, 1995: Dual-doppler and multiparameter radar observations of a bow-echo hailstorm. Mon. Wea. Rev., 123, 921-943.

Kerr, B.W., and G.L. Darkow, 1996: Storm-relative winds and helicity in tornadic thunderstorm environments. *Wea. Forecasting*, **11**, 489-505.

Klemp, J.B., 1987: Dynamics of tornadic thunderstorms. *Ann. Rev. Fluid Mech*., **19**, 369-402.

Kaplan, M.L., J.W. Zack, V.C. Wong, and G.D. Coats, 1984: The interactive role of subsynoptic scale jet streak and planetary boundary layer processes in organizing an isolated convective complex. *Mon. Wea. Rev.*, **112**, 2212-2238.

Koch, S.E., and J. M. McCarthy, 1982: The evolution of an Oklahoma dryline. Part II: Boundary- layer forcing of mesoconvective systems. *J. Atmos. Sci*., **39**, 237-257.

____, C. A. Ray, 1997: Mesoanalysis of summertime convergence zones in central and eastern North Carolina. *Wea. Forecasting*, **12**, 56–77

Lee, B.D. and R. Wilhelmson, 1996: Visualization of a numerically simulated family of "landspout" tornadoes along a weak outflow boundary. Video and accompanying text, produced at the Univ. of Illinois at Urbana-Champaign, Dept. of Atmospheric Science.

Lemon, L.R., 1980: Severe thunderstorm radar identification techniques and warning criteria. NOAA Tech. Memo. NWS NSSFC-3, 60 pp.

Lemon, L.R., R.J. Donaldson, D.W. Burgess, and R.A. Brown, 1977: Doppler radar application to severe thunderstorm study and potential real-time warning. *Bull. Amer. Meteor. Soc*., **58**, 1187-1193.

Maddox, R. A., 1976: An evaluation of tornado proximity wind and stability data. *Mon. Wea. Rev.*, **104**, 133–142.

____, C.F. Chappell, and L.R. Hoxit, 1979: Synoptic and mesoscale aspects of flash flood events. *Bull. Amer. Meteor. Soc.*, **60**, 115-123.

____, 1980: Mesoscale convective complexes. *Bull. Amer. Meteor. Soc.*, **61**, 1374-1387.

____, 1983: Large-scale meteorological conditions associated with midlatitude, mesoscale convective complexes. *Mon. Wea. Rev.*, **111**, 1475-1493.

Mahoney, W.P. III, 1988: Gust front characteristics and the kinematics associated with interacting thunderstorm outflows. *Mon. Wea. Rev.*, **116**, 1474-1491.

Markowski, P.M., E. M. Rasmussen, and J.M. Straka, 1998: The occurrence of tornadoes in supercells interacting with boundaries in VORTEX-95. *Wea. Forecasting*, **13**, 852-859.

Marwitz, J.D., 1972a: The structure and motion of severe hailstorms. Part I: Supercell storms. *J. Appl. Meteor.*, **11**, 166-179.

____, 1972b: The structure and motion of severe hailstorms. Part II: Multi-cell storms. *J. Appl. Meteor.*, **11**, 180-188.

____, 1972c: The structure and motion of severe hailstorms. Part III: Severely sheared storms. *J. Appl. Meteor.*, **11**, 189-201.

____, and A. Auer, 1972: Hail in the vicinity of organized updrafts. *J. Appl. Meteor.*, **11**, 748-752.

McCaul, E. W., Jr., 1991: Buoyancy and Shear characteristics of hurricane-tornado environments. *Mon Wea. Rev.* **119**, 1954-1978.

McCaul, E. W., and M. L. Weisman, 1996: The dependence of simulated storm structure on variations in the shapes of environment buoyancy and shear profiles. Preprints, *18th Conf. on Severe Local Storms*, San Francisco, CA, Amer. Meteor. Soc., 718-722.

McCann, D.W., 1994: WINDEX – a new index for forecasting microburst potential. *Wea. Forecasting*, **9**, 532.

Moller, A.R., C.A. Doswell III, and R. Przybylinski, 1990: High-precipitation supercells: A conceptual model and documentation. Preprints, *16th Conf. on Severe Local Storms*, Kananaskis Park, Alta., Canada, Amer. Meteor. Soc., 52-57.

Moller, A.R., C.A. Doswell III, M.P. Foster, and G.R. Woodall, 1994: The operational recognition of supercell thunderstorm environments and storm structures. *Wea. Forecasting*, **9**, 327-347.

Moncrieff, M. W., and Liu, C. 1999. Convection initiation by density currents: Role of convergence, shear, and dynamical organization. *Mon. Wea. Rev*. **127**, 2455–2464.

Monteverdi, J.P., 1993: A Case Study of the Operational Usefulness of the SHARP Workstation in Forecasting a Mesocyclone-Induced Cold Sector Tornado Event in California. NOAA Tech. Memo. WR-219, 22 pp.

Monteverdi, J.P., and J. Quadros, 1993: Convective and Rotational Parameters Associated with Three Tornado Episodes in Northern and Central California. NOAA Tech. Memo. WR-222, 23 pp.

Newton, C.W., 1967: Severe Convective Storms. *In Advances in Geophysics, Vol. 12*, Academic Press, 257-303.

Petersen, W.r A., L. D. Carey, S. A. Rutledge, J. C. Knievel, R. H. Johnson, N. J. Doesken, T. B. McKee, T. Vonder Haar, and J. F. Weaver, 1999: Mesoscale and Radar Observations of the Fort Collins Flash Flood of 28 July 1997. *Bull. Amer. Meteor. Soc*., **80**, 191–216.

Przybylinski, R.W., 1995: The bow echo: observations, numerical simulations, and severe weather detection methods. *Wea. Forecasting*, **10**, 203-218.

____, 1995: The bow echo: Observations, numerical simulations, and severe weather detection methods. *Wea. Forecasting*, **10**, 203-218.

____, and G.K. Schmocker, 1993: The evolution of a widespread convective wind storm event over central and eastern Missouri. Preprints, *13th Conf. on Weather Analysis and Forecasting*, Vienna, VA, Amer. Meteor. Soc., 461-465.

____, T.J. Shea, D.L. Ferry, E.H. Goetsch, R.R. Czys, and N.E. Wescott, 1993: Doppler radar observations of high-precipitation supercells over the mid-Mississippi Valley region. Preprints, *17th Conf. on Severe Local Storms*, St. Louis, MO, Amer. Meteor. Soc., 158-163.

____., and D. M. DeCaire, 1985: Radar signatures associated with the derecho. One type of mesoscale convective system. Preprints *14th Conf. on Severe Local Storms*, Indianapolis, IN, Amer. Meteor. Soc., 228-231.

Purdom, J. F. W., 1976: Some uses of high resolution GOES imagery in the mesoscale forecasting of convection and its behavior. *Mon. Wea. Rev.*, 104, 1474–1483

RTM-230, 2000: Skew T Log P Diagram and Sounding Analysis, National Weather Service Training Center Remote Training Module.

Rasmussen, E. N., 2001: Refined supercell and tornado forecast parameters from the 1992 baseline climatology. Unpublished web-based paper.

____, and D. Blanchard, 1998: A baseline climatology of sounding-derived supercell and tornado forecast parameters. *Wea and Forecasting*, **13**, 1148-1164.

____, S. Richardson, J. Straka, P. Markowski, and D. Blanchard, 1998: The association of significant tornadoes with a baroclinic boundary on 2 June 1995. *Mon. Wea. Rev.*, **128**, 174-191.

____, and J. Straka, 1997: Variations in Supercell Morphology. Part I: Observations of the Role of Upper-Level Storm-Relative Flow. *Mon. Wea. Rev.*, **126**, 2406-2421.

____, and R. B. Wilhelmson 1983: Relationships between storm characteristics and 1200 GMT hodographs, low-level shear, and stability. preprints, *13th conf. on Severe Local Storms,* Tulsa, OK, Amer. Meteor. Soc., J5-J8.

Richardson, Y.P., 1999: The Influence of horizontal variations in vertical shear and low-level moisture on numerically simulated convective storms. Ph.D. Dissertation, School of Meteorology, University of Oklahoma - Norman, 236 pp.

Rotunno, R., 1993: Supercell thunderstorm modeling and theory. *Geo. Monograph* **79**, 57--73.

____, and J.B. Klemp, 1982: The influence of the shear-induced pressure gradient on thunderstorm motion. Mon. Wea. Rev., 110, 136-151.

____, and J. Klemp, 1985: On the rotation and propagation of simulated supercell thunderstorms. *J. Atmos. Sci*., **42**, 271-292.

____, J. B. Klemp, and M. L. Weisman, 1988: A theory for strong, long-lived squall lines. *J. Atmos. Sci.*, **45**, 463–485.

Schmocker, and Y.Lin, 1999: Storm Reflectivity and Mesocyclone Evolution Associated with the 15 April 1994 Squall Line over Kentucky and Southern Indiana. *Wea. Forecasting*, **14**, 976—993.

Shapiro, A. 1992. A hydrodynamical model of shear flow over semi-infinite barriers with application to density currents. *J. Atmos. Sci*. **49**, 2293–2305

Smull, Bradley F., R. A. Houze, Jr., 1987: Rear Inflow in Squall Lines with Trailing Stratiform Precipitation. Mon. Wea. Rev., 115, 2869–2889.

Stensrud, D.J., J.V. Cortinas, Jr., and H.E. Brooks, 1997: Discriminating between tornadic and nontornadic thunderstorms using mesoscale model output. *Wea. Forecasting*, **12**, 613-632.

Thompson, R.L., 1996: Supercell tornado forecasts derived from Eta model storm-relative winds. Preprints, *18th Conf. on Severe Local Storms*, San Francisco, CA, AMS, 362-366.

____, 1998: Eta model storm-relative winds associated with tornadic and nontornadic supercells. *Wea. Forecasting*, **13**, 125-137.

Vasiloff, S.V., E.A. Brandes, R.P. Davies-Jones, and P.S. Ray, 1986: An investigation of the transition from multicell to supercell storms. *J. Climate and Appl. Meteor.*, **25**,1022-1036.

Weaver, J. F., 1979: Storm Motion as Related to Boundary-Layer Convergence. *Mon. Wea. Rev.*, **107**, 612–619.

Weisman, M. L., 1996: On the use of vertical wind shear versus helicity in interpreting supercell dynamics. Preprints, *18th Conf. on Severe Local Storms*, San Francisco, CA, Amer. Meteor. Soc., 200-204.

____, 1993: The Genesis of Severe, Long-Lived Bow Echoes. *J. Atmos. Sci.*, **50**, 645–645.

____, 1992: The Role of Convectively Generated Rear-Inflow Jets in the Evolution of Long-Lived Mesoconvective Systems. *J. Atmos. Sci.*, **49**, 1826–1847.

____, and J. B. Klemp, and R. Rotunno, 1988: Structure and evolution of numerically simulated squall lines. *J. Atmos. Sci.*, **45**, 1990-2013.

____, and J. B. Klemp, 1986: Characteristics of isolated convective storms. Mesoscale Meteorology and Forecasting, P.S. Ray, Ed., Amer. Meteor. Soc., 331-358.

_____, and H.B. Bluestein, 1985: Dynamics of numerically simulated LP storms. Preprints, *14th Conf. on Severe Local Storms*, Indianapolis, IN, Amer. Meteor. Soc., 167-170.

____., and J. B. Klemp, 1984: The structure and classification of numerically simulated convective storms in directionally varying wind shears. *Mon. Wea. Rev.*, **112**, 2479-2498.

___, J. B. Klemp, and J. W. Wilson, 1983: Dynamic interpretation of notches, WERS, and mesocyclones simulated in a numerical cloud model. Preprints, *21st Conf. on Radar Meteorology*, Edmonton, Alta., Canada, Amer. Meteor. Soc., 39-43.

____, and J. B. Klemp, 1982: The dependence of numerically simulated convective storms on vertical wind shear and buoyancy. *Mon. Wea. Rev.*, **110**, 504-520.

Wicker, L. J., and L. Cantrell, 1996: The role of vertical buoyancy distributions in miniature supercells. Preprints, *18th Conf. on Severe Local Storms*, San Francisco, CA, Amer. Met. Soc, 225-229.

Wilson, J.W., 1986: Tornadogenesis by nonprecipitation induced wind shear lines. *Mon. Wea. Rev.*, **114**, 270-284.

____, R. E. Carbone, J. D. Tuttle, and T. D. Keenan, 2001: Tropical island Convection in the Absence of Significant topography. Part II: Nowcasting Storm Evolution. *Mon. Wea. Rev.*, **129**, 1507–1525.

____, and D. L. Megenhardt, 1997: Thunderstorm Initiation, Organization, and Lifetime Associated with Florida Boundary Layer Convergence Lines. *Mon. Wea. Rev*. **125**, 1507–1525

____, and W. E. Schreiber, 1986: Initiation of convective storms by radar-observed boundary layer convergent lines. *Mon. Wea. Rev.*, **114**, 2516—2536

Xue, M. 2000. Density currents in two-layer shear flows. *Quart. J. Roy. Atmos. Sci.*, **126**, 1301—1320.

Zhang, D., 1992: The formation of a cooling-induced mesovortex in the trailing stratiform region of a midlatitude squall line. *Mon. Wea. Rev.*, **120**, 2763-2785.

Zipser, E.J., 1982: Use of a conceptual model of the life cycle of mesoscale convective systems to improve very-short-range forecasts. In Nowcasting, K.A. Browning (Ed.), Academic Press, 191-204.

102 Bibliography